Multigrid line smoothers for higher order upwind discretizations of convection-dominated problems

C.W. Oosterlee *, F.J. Gaspar, ‡ T. Washio §and R. Wienands *

AMS(MOS) 65N20, 65N55, 76D05

Keywords: multigrid, line smoothers, higher order discretizations, convection domination.

*GMD, Institute for Algorithms and Scientific Computing) ,
D-53754 Sankt Augustin, Germany
(email: oosterlee @ gmd.de),(wienands@gmd.de)

‡C.P.S. University of Zaragoza 50008 Zaragoza, Spain
(email: fjgaspar @ mcps.unizar.es)

§C&C Research Laboratories, NEC Europe Ltd., D-53757 Sankt Augustin, Germany
(email: washio @ ccrl-nece.technopark.gmd.de)

Proposed running head: Line smoothers for convection-dominated problems

Mailing address:
Dr. C.W. Oosterlee,
GMD.SCAI,
Schloss Birlinghoven
D-53754 Sankt Augustin
Germany
tel: (+49) 2241 14 2118
fax: (+49) 2241 14 2460
email: oosterlee@gmd.de

Multigrid line smoothers for higher order upwind discretizations of convection-dominated problems

C.W. Oosterlee, F.J. Gaspar, T. Washio and R. Wienands

Abstract:

In this paper we present new multigrid line smoothers for the solution of higher order discretizations of scalar convection-dominated problems directly. The behavior of the smoothers is analyzed theoretically with Fourier smoothing and two-grid analysis. A parallel tri-line variant is presented and evaluated. The smoothers are applied to scalar convection-diffusion problems, discretized with limiters and systems of incompressible Navier-Stokes and Euler equations.

1 Introduction

Multigrid methods are generally accepted as fast efficient solution methods, especially for elliptic problems when the discretization results in an M-matrix [22]. For these problems, basic iterative methods, like point or line Gauss-Seidel methods are not satisfactory solvers, but they are efficient *smoothers*. This means that instead of solving all frequencies of the error components, they efficiently reduce the high frequency components and therefore smooth the error between numerical and exact solution. A smoother is one essential part of a multigrid method. The other part is the coarse grid correction, which is based on the knowledge that a smooth error can be well represented on coarser grids. On a coarser grid a smoother can then reduce the "high" frequencies corresponding to this grid. By repeating this procedure on several grids, the multigrid solution method is obtained. More details on multigrid can be found in [2], [10], [20] and [24]. The multigrid method is also commonly used for singularly perturbed problems, like convection-dominated (systems of) equations. Here, the error is not only smoothed, it is also reduced along the characteristic direction of a convection operator. For these problems, however, good smoothers are not necessarily the same ones as in the full elliptic case. Basic iterative methods with grid point ordering "against the flow", for example, do not smooth the error. Also the quality of a smoother depends on the discretization used for the convection terms. Efficient smoothers for convection-dominated problems are the main topic of this paper.

Higher order finite difference or finite volume discretizations of convection-dominated problems, on the basis of van Leer's κ-schemes [21], do not result in M-matrices and their multigrid treatment is not as efficient as for Poisson-like problems.
Usually, κ-scheme discretizations are solved indirectly with a defect correction technique, where multigrid is used for solving the first order discretization. The higher order discretization scheme is then used as an outer iteration. In the defect correction approach often the outer iteration determines the convergence speed, which can be slow if the first and higher order discretizations are very different.

A second popular approach, in which higher order discretizations are solved directly in multigrid, is with the help of multistage smoothers [12], [24]. These smoothers are point smoothers of Jacobi type and are therefore limited in their robustness with respect to problems discretized on grids with stretched cells.

In this paper, instead of the two approaches mentioned above, a robust alternative is presented, in which the higher order upwind discretization is also solved directly in multigrid. We present line smoothers based on a splitting of the operator into a 'positive' part on the left-hand side and the remaining part on the right-hand side. Positive parts (a positive main diagonal and nonpositive off diagonal elements) are required in the left-hand side, in order to assure a splitting to have smoothing properties. The smoothers based on this splitting can be of alternating, symmetric or zebra type and are called KAPPA smoothers here.
The resulting splitting is analyzed with Fourier smoothing analysis [2] for a linear convection diffusion equation discretized with the κ-scheme, similar to Wesseling [24] (for the standard upwind discretization). Furthermore, two-grid Fourier analysis [20], [5] is applied.
A parallel variant is a tri-line zebra smoother, due to the fact that a higher order 1D upwind stencil contains 4 elements. It is evaluated, whether the parallel smoother is an interesting competitor for the robust (non parallel) symmetric alternating line smoother. In Section 2.1 we will briefly describe the discretization of the convective terms. In Section 2.2 the multigrid solution method with the new splitting for the line smoothers is introduced. The theoretical results are

compared to the actual multigrid convergence for model problems in Section 3. In the two-grid analysis we observe the discrepancy between the scaling of convection and diffusion on fine and coarse grids, as is studied in [4], [3] and mentioned in [5]. For the 'inflow/outflow' problems evaluated here we will not see the negative effect of the different scaling on the multigrid convergence, due to the influence of the combination of Dirichlet boundary conditions and the line smoothers, which reduce not only high frequency, but also low frequency error components. Overweighting of residuals [4], or a Krylov acceleration [15] as a way to improve the convergence (mainly for rotating convection-dominated problems) is not needed here and therefore not adopted.
The multigrid solution method used here is the nonlinear FAS [2] scheme, because we will also investigate the influence on the multigrid convergence of discretization schemes with limiters. Discretizations with limiters lead to nonlinear discretizations, even for linear problems. Numerical tests for linear and nonlinear convection-dominated scalar problems are performed on fine grids in Section 5, where the new method is compared with the defect correction approach. Furthermore, the smoothers are tested for systems of incompressible Navier-Stokes and compressible Euler equations.

2 The discretization and the solution method

2.1 Higher order upwind discretization of a convection term

We consider a linear variant of the convection-diffusion equation:

$$L\phi = (a\,\phi)_x + (b\,\phi)_y - \epsilon\,\Delta\phi = f \tag{1}$$

where $0 < \epsilon << 1$, Δ denotes the Laplacian, a, b and f are given functions possibly depending on x and y. We discretize (1) on a grid with mesh size $h_x = h_y = h$. The diffusion term is approximated with the standard five point approximation. For the convection terms $(a\phi)_x$ and $(a\phi)_y$, we distinguish between a different upwind approximations. In general a good discretization for convection should obey two important requirements:

1 The discretization should be $O(h^2)$ accurate (at least for "smooth" parts of a solution).

2 The discretization should be monotone. This means that a solution should not contain wiggles, spurious oscillations that results in local unphysical extrema.

The standard upwind discretization for $(a\phi)_x$ looks (for $a = const > 0$) like:

$$(a\phi)_x = \frac{a}{h}(\phi_{i,j} - \phi_{i-1,j}) =: L_1 \tag{2}$$

However, it is well-known that this discretization scheme is only $O(h)$ accurate. A first choice for obtaining second order accurate schemes with a linear discretization is the class of κ-schemes, which work satisfactorily for a large class of CFD problems including the incompressible Navier-Stokes equations. The κ-schemes are, however, not monotone, which means that they have to be modified (with limiters) for CFD problems containing strong gradients or boundary layers. κ-schemes result in a linear discretization, which enables them to be easily analyzed (for example with Fourier analysis). The discretization of $(a\phi)_x$ with van Leer's κ-scheme [21] looks (for $a = const > 0$) like:

$$\begin{aligned}(a\phi)_x &= \frac{a}{h}[(\phi_{i,j} - \phi_{i-1,j}) - \frac{\kappa}{2}(\phi_{i,j} - \phi_{i-1,j}) + \frac{1+\kappa}{4}(\phi_{i+1,j} - \phi_{i,j}) - \frac{1-\kappa}{4}(\phi_{i-1,j} - \phi_{i-2,j})] \\ &= L_1 + L_\alpha + L_\beta + L_\gamma \end{aligned} \tag{3}$$

For $a < 0$ similar formulae are found, and the evaluation of ϕ_y is straightforward. Furthermore, if $a = a(x,y) \neq const$, (3) is easily changed by introducing $a_{i+1/2,j}$ and $a_{i-1/2,j}$ in a standard finite difference or volume discretization. The resulting discretization obtained with the κ-scheme is denoted by L_2. The stencil for (1) with (3), $(a, b = const > 0)$ and $\kappa = 0$ (called Fromm's scheme) looks like:

$$[L_2] = \frac{a}{h}[1/4 \quad -5/4 \quad 3/4 \quad 1/4 \quad 0] + \frac{b}{h}\begin{bmatrix} 0 \\ 1/4 \\ 3/4 \\ -5/4 \\ 1/4 \end{bmatrix} + \frac{\epsilon}{h^2}\begin{bmatrix} 0 & -1 & 0 \\ -1 & 4 & -1 \\ 0 & -1 & 0 \end{bmatrix} \tag{4}$$

The Fromm scheme is second order accurate, whereas the Cubic Interpolation Upwind (CUI) scheme ($\kappa = 1/3$) [1] is formally third order accurate in space, which can be confirmed by Taylor's expansion.
It can be seen from (4) that κ-discretizations in general do not result in M-matrices [22], for which it is well-known that basic iterative methods, like Gauss-Seidel, are convergent methods. Using the basic iterative methods as a smoother directly on L_2 leads actually to a *diverging* method. For multigrid smoothers it is essential that the discretization is taken into account. Positive parts $L_1 + L_\alpha$ of the second order discretization (3) will be used in the left-hand side. Positive parts (a positive main diagonal and nonpositive off diagonal elements) are required in the left-hand side, in order to assure it to be invertible. Positivity is the point of departure for every smoothing method known.

As already mentioned, discretizations with κ-schemes produce unphysical oscillations near sharp gradients or discontinuities in a solution. Therefore, Total Variation Diminishing (TVD) concepts have been introduced, preventing a solution from oscillating. An overview of the TVD schemes is given in [11] and also in [25]. The basis for the so-called monotone TVD discretizations is the introduction of limiters. Limiters result in nonlinear discretizations even for linear problems. We will evaluate the multigrid convergence for discretizations with different limiters. A good starting point for the discretization with limiters is the discretization of (1) with (3) and $\kappa = -1$, the second order upwind scheme, which looks (for $a > 0$) like:

$$(a\phi)_x = \frac{a}{h}[(\phi_{i,j} - \phi_{i-1,j}) + \frac{1}{2}(\phi_{i,j} - \phi_{i-1,j}) - \frac{1}{2}(\phi_{i-1,j} - \phi_{i-2,j})] = L_1 + L_\alpha + L_\gamma \tag{5}$$

The second order upwind scheme is introduced as a first order upwind scheme L_1 plus additional terms L_α and L_γ. (Again a similar splitting is found for $a < 0$ or for a and b functions depending on x and y.) To satisfy TVD conditions the additional terms L_α and L_γ are multiplied by limiters, which are functions of the ratio of local differences of unknowns:

$$\begin{aligned} (a\phi)_x &= \frac{a}{h}[(\phi_{i,j} - \phi_{i-1,j}) + \frac{1}{2}\Psi(R_{i-1/2})(\phi_{i,j} - \phi_{i-1,j}) - \frac{1}{2}\Psi(R_{i-3/2})(\phi_{i-1,j} - \phi_{i-2,j})] \\ &= \qquad L_1 + \qquad\qquad L_\alpha + \qquad\qquad L_\gamma \end{aligned} \tag{6}$$

Here, $R_{i-1/2} \equiv (\phi_{i+1,j} - \phi_{i,j})/(\phi_{i,j} - \phi_{i-1,j})$ and $R_{i-3/2} \equiv (\phi_{i,j} - \phi_{i-1,j})/(\phi_{i-1,j} - \phi_{i-2,j})$.
It is well-defined in which region in a $(R, \Psi(R))$-diagram the limiting function $\Psi(R)$ should lie, so that the resulting convection discretization is monotone and higher order accurate ([11], [25]) (also shown in Figures 1 and 2). In recent years many limiters have been proposed and evaluated, since for every problem (compressible equations with shocks, turbulence modeling,

etc.) a corresponding best limiter can be constructed. Here we sum up some of these limiters for which we investigate the multigrid convergence. Investigations on accuracy with limiters for model problems and applications is done in many other papers.

We distinguish two classes of limiters. For the first class of limiters we will present a robust convergence improvement in Section 4. The limiters in this class do not follow parts of the line $\Psi(R) = 2R$ in the $(R, \Psi(R))$-plane. Some well-known limiters in this class are:

$$\Psi(R) = \frac{R^2 + R}{R^2 + 1} \qquad \textit{Van Albada limiter} \tag{7}$$

$$\Psi(R) = \frac{|R| + R}{R + 1} \qquad \textit{Van Leer limiter} \tag{8}$$

$$\Psi(R) = \frac{(|R| + R)(3R + 1)}{2(R + 1)^2} \qquad \textit{ISNAS limiter } [25] \tag{9}$$

(The limiters for which we do not give an explicit reference are well-known and can be found in [11], [25]). The limiters (7), (8) and (9) are presented in a $(R, \Psi(R))$-diagram in Figure 1. It

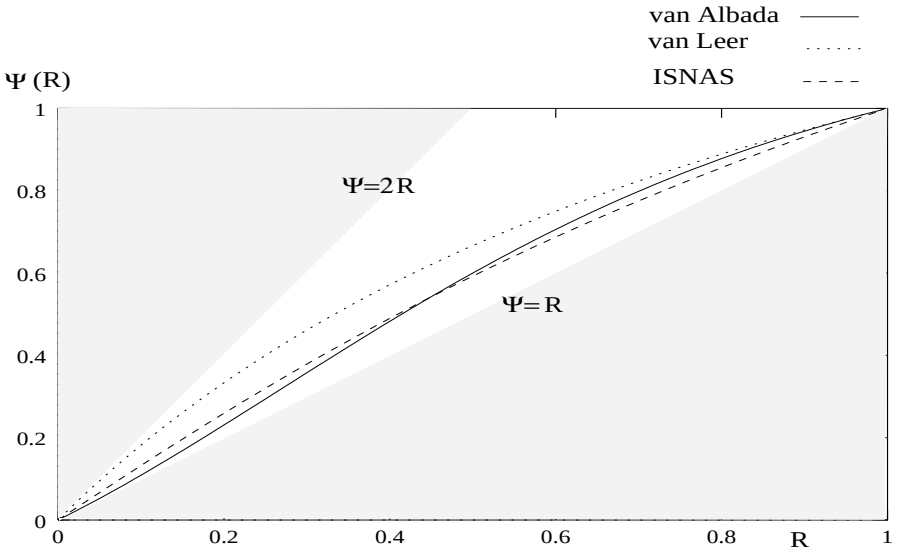

Figure 1: Three limiters and the monotonicity region in a $(R, \Psi(R))$-diagram.

can be seen that for all the limiters examined (6) is identical to (5) for $R = 1$, which ensures second order accuracy in smooth regions.
The second class of limiters is the class of *strong compressive* limiters, whose function values are $2R$ near the origin in the $(R, \Psi(R))$-diagram. Examples are the Superbee limiter, the SMART limiter and the limited $\kappa = 1/3$ scheme:

$$\Psi(R) = \max[0, \min(2R, 1), \min(R, 2)] \quad \textit{Superbee limiter} \tag{10}$$

$$\Psi(R) = \max[0, \min(4, \tfrac{3}{4}R + \tfrac{1}{4}, 2R)] \quad \textit{SMART limiter } [8] \tag{11}$$

$$\Psi(R) = \max[0, \min(2, \tfrac{2}{3}R + \tfrac{1}{3}, 2R)] \quad \kappa = 1/3 \ \textit{limiter } [14] \tag{12}$$

These limiters are shown in Figure 2. When the values from $2R$ are chosen the resulting dis-

cretization for $a > 0$ becomes:

$$(a\phi)_x = \frac{a}{h}[-\phi_{i,j} + \phi_{i+1,j}] \tag{13}$$

The negative main diagonal element already indicates that fast convergence with iterative methods for the steady equation discretized with a limiter from class 2 might not be trivial.

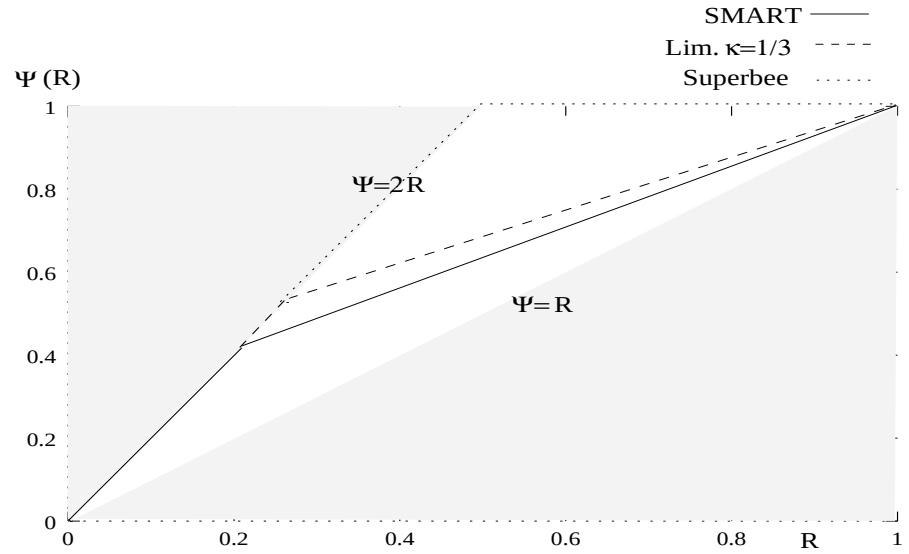

Figure 2: Three '$2R$'-limiters (they follow the function $\Psi = 2R$ near the origin) and the monotonicity region in a $(R, \Psi(R))$-diagram.

As in (5), it can be seen from (6) and from the definition of the limiters, that L_α in (6) is always positive.

Boundary discretization. The schemes used here employ more than nearest neighbors, which means that special care is needed near boundaries. We discretize the first line of cells near a boundary with the central difference scheme ($\kappa = 1$). In the numerical experiments, it was found really necessary to use second order accurate schemes near boundaries in order to keep the overall accuracy. Wiggles, spurious oscillations due to the central differencing were never observed in the test examples evaluated.

2.2 The multigrid solution method

A general representation of $L_2\phi$ looks like:

$$L_2\phi = \sum_{\mu_x \in J} \sum_{\mu_y \in J} a^{(2)}_{\mu_x \mu_y} \phi_{i+\mu_x, j+\mu_y} \,, \tag{14}$$

with coefficients $a^{(2)}_{\mu_x \mu_y}$ coming for the second order κ formulation or from a linearization (in our case Picard) of the limited formulation and a set of indices $J = \{-2, -1, 0, 1, 2\}$. By using the

stencil notation L_2 can be rewritten as

$$L_2 = \begin{pmatrix} & & a^{(2)}_{02} & & \\ & & a^{(2)}_{01} & & \\ a^{(2)}_{-20} & a^{(2)}_{-10} & a^{(2)}_{00} & a^{(2)}_{10} & a^{(2)}_{20} \\ & & a^{(2)}_{0-1} & & \\ & & a^{(2)}_{0-2} & & \end{pmatrix} \tag{15}$$

We will solve the discretization from (15) directly with a multigrid solution method. Here, we will introduce two splittings for which it will be shown in the next section that they are robust smoothers for discretizations with (3).
The first splitting introduced is a robust smoother for large κ-range (linear κ-scheme): $-1 \leq \kappa \leq 0.8$;
The second splitting is robust for a smaller κ-range $-0.3 \leq \kappa \leq 0.5$, but it is easier to program for systems of equations. Both splittings are not good smoothers for values of κ near 1 (the central difference scheme).
All multigrid components, except the smoother, are standard components, which we will not discuss in detail. The restriction operator is the Full Weighting operator ([20]); the prolongation is bi-linear interpolation. The discretization on the coarse grids is the direct discretization from the differential equation on the coarse grid. For problems with discontinuities and the discretization with limiters we will see that it is worth comparing the L_2 discretization on coarse grids, called *full second order formulation* in [7], [19] with the L_1 discretization on coarse grids, called *mixed discretization formulation* [7].

Smoother. The *robust* smoother we will introduce is of alternating symmetric type. Lines are processed in x- and y-directions in forward and backward lexicographical ordering. This smoother is denoted as $S = S^{y_b} S^{y_f} S^{x_b} S^{x_f}$. For particular problems it is of course possible to choose the direction of line smoothing 'with the flow'. A parallelizable variant is explained at the end of this subsection.
A part of the robust smoother, the x-line sweep for a forward ordering of grid lines, S^{x_f}, is explained in detail. The derivation of the other parts is straightforward. For S^{x_f}, L_2 (15) is split as follows:

$$L_2 = L^x_{1/2} - (L^x_{1/2} - L_2) =: L^+ + L^0 - (-L^-) \qquad \text{with} \tag{16}$$

$$L^x_{1/2} := L^+ + L^0 = \begin{pmatrix} & & 0 & & \\ & & 0 & & \\ 0 & 0 & 0 & 0 & 0 \\ & & a^{(2)}_{0-1} & & \\ & & a^{(2)}_{0-2} & & \end{pmatrix} + \begin{pmatrix} & & 0 & & \\ & & 0 & & \\ 0 & a^{(1/2)}_{-10} & a^{(1/2)}_{00} & a^{(1/2)}_{10} & 0 \\ & & 0 & & \\ & & 0 & & \end{pmatrix} \tag{17}$$

$$\Rightarrow L^x_{1/2}\phi^{m+1} = (L^x_{1/2} - L_2)\phi^m + f \tag{18}$$

The $a^{(1/2)}_{**}$ elements in (17) are the positive parts $L_1 + L_\alpha$ or L_1 in the discretizations (3),(6) to be discussed below. The two splittings differ in the way that coefficients $a^{(1/2)}_{**}$ are defined. We call the smoothers based on both splittings "KAPPA smoothers" here.
Splitting 1: The coefficients $a^{(1/2)}_{**}$ include the first order upwind operator L_1, plus a 'positive' part of the second order operator: L_α in (3), (5) or (6) plus the parts of the diffusion operator.

Splitting 2: The coefficients $a_{**}^{(1/2)}$ correspond only to the first order upwind operator L_1 (2) of a discretized equation (plus the parts of the diffusion operator). The smoother from Splitting 2 is less robust, but it is more general applicable, since a first order upwind discretization is in the left-hand side and the remaining part is in the right-hand side. Other (point) smoothers in the literature (for example in [19]) for second order discretizations are more often based on Splitting 2.
Other splittings, based on rewriting (6) like [11]:

$$(a\phi)_x = \frac{a}{h}\left[1 + \frac{1}{2}\Psi(R_{i-1/2}) - \frac{1}{2}\frac{\Psi(R_{i-3/2})}{R_{1-3/2}}\right](\phi_{i,j} - \phi_{i-1,j})$$

did not lead to better line smoothers, although the coefficient between square brackets is also guaranteed to be positive by the properties of limiters.

Choosing the $i \pm 2$ variables also in L^0 gives us another alternative, which does not satisfy the positivity rule. This smoother, resulting in a pentadiagonal solver instead of the tridiagonal solver, is not considered here.

The meaning of the superscripts $\{-, 0, +\}$ in (16) is clear when we consider (18) for a fixed line $(i, j_0)_{1 \le i \le n}$:

$$L^0\phi^* = f + L^0\phi^m - (\,(L^- + L^0)\phi^m + L^+\phi^{m+1}\,) \tag{19}$$

L^0 corresponds to the unknowns which are smoothed simultaneously. L^- is applied to the old approximation ϕ^m and for L^+ new values are already available ([20]), which is dictated by the ordering of the grid lines. Inserting an underrelaxation parameter ω in (19) leads to:

$$\phi^{m+1} = \omega\phi^* + (1-\omega)\phi^m \tag{20}$$

With $\omega = 1$ we regain (18). We can rewrite (19) in the correction formulation, where during the smoothing iteration a correction $\delta\phi^{m+1}$ is calculated, which is then added to the current approximation with underrelaxation parameter ω:

$$\begin{aligned} L^0\delta\phi^{m+1} &= f - ((L^- + L^0)\phi^m + L^+\phi^{m+1}) \\ L^0\delta\phi^{m+1} &= f - L_2\phi^{m+1/2} \qquad (21) \\ \phi^{m+1} &= \phi^m + \omega\delta\phi^{m+1} \qquad (22) \end{aligned}$$

In (21) operator L_2 is appearing in the right-hand side, and $\phi^{m+1/2}$ denotes ϕ^m or ϕ^{m+1}: it is the latest value available.
As an example and in order to explain the difference between Splitting 1 and Splitting 2, we determine $L^0\phi$, $L^-\phi$ and $L^+\phi$ for $a > 0$ and $b > 0$ in (1), (the example we discussed in detail in Section 2.1). For the x-line KAPPA smoother S^{x_f} from Splitting 1, we then find with (2), (3):

$$\begin{aligned} L^0\phi &= \left[-\frac{a}{h}\left(\frac{2-\kappa}{2}\right) - \frac{\epsilon}{h^2}\right]\phi_{i-1,j} + \left[\frac{a}{h}\left(\frac{2-\kappa}{2}\right) + \frac{4\epsilon}{h^2} + \frac{b}{h}\left(\frac{2-\kappa}{2}\right)\right]\phi_{i,j} + \left[-\frac{\epsilon}{h^2}\right]\phi_{i+1,j} \\ L^+\phi &= \left[\frac{b}{h}\left(\frac{1-\kappa}{4}\right)\right]\phi_{i,j-2} + \left[-\frac{b}{h}\left(\frac{5-3\kappa}{4}\right) - \frac{\epsilon}{h^2}\right]\phi_{i,j-1} \\ L^-\phi &= \left[\frac{a}{h}\left(\frac{1-\kappa}{4}\right)\right]\phi_{i-2,j} + \left[\frac{a}{h}\left(\frac{\kappa-1}{4}\right)\right]\phi_{i-1,j} + \left[-\frac{a+b}{h}\left(\frac{1+\kappa}{4}\right)\right]\phi_{i,j} + \\ &\quad \left[\frac{a}{h}\left(\frac{1+\kappa}{4}\right)\right]\phi_{i+1,j} + \left[\frac{b}{h}\left(\frac{1+\kappa}{4}\right) - \frac{\epsilon}{h^2}\right]\phi_{i,j+1} \end{aligned} \tag{23}$$

From Splitting 2 we obtain:

$$
\begin{aligned}
L^0\phi &= \left[-\frac{a}{h}-\frac{\epsilon}{h^2}\right]\phi_{i-1,j}+\left[\frac{a}{h}+\frac{4\epsilon}{h^2}+\frac{b}{h}\right]\phi_{i,j}+\left[-\frac{\epsilon}{h^2}\right]\phi_{i+1,j}\\
L^+\phi &= \left[\frac{b}{h}\left(\frac{1-\kappa}{4}\right)\right]\phi_{i,j-2}+\left[-\frac{b}{h}\left(\frac{5-3\kappa}{4}\right)-\frac{\epsilon}{h^2}\right]\phi_{i,j-1}\\
L^-\phi &= \left[\frac{a}{h}\left(\frac{1-\kappa}{4}\right)\right]\phi_{i-2,j}+\left[-\frac{a}{h}\left(\frac{1-3\kappa}{4}\right)\right]\phi_{i-1,j}+\left[-\frac{a+b}{h}\left(\frac{1+3\kappa}{4}\right)\right]\phi_{i,j}+\\
&\quad \left[\frac{a}{h}\left(\frac{1+\kappa}{4}\right)\right]\phi_{i+1,j}+\left[\frac{b}{h}\left(\frac{1+\kappa}{4}\right)-\frac{\epsilon}{h^2}\right]\phi_{i,j+1} \qquad (24)
\end{aligned}
$$

Notice that both splittings are identical for $\kappa = 0$.

Remark: Note that the smoothers explained here for diffusion-dominant problems, or for problems with diffusion and convection of the same size are well-known line smoothers, resulting in excellent multigrid convergence rates.

A parallel variant. The symmetric alternating line smoother is a sequential smoother. The right-hand side of a new line j_0 (19) to be processed depends on just updated ϕ values of lines j_0-1 and j_0-2 (or j_0+1 and j_0+2). In order to have a parallel smoother, it is desirable that this dependency is minimized. One possible way is by processing the lines in a Jacobi type iteration: only old values ϕ^m are then appearing in the right-hand side of (19) and L^+ is empty. However, experience has shown that Jacobi smoothers are often less efficient than smoothers in which recent values are used for new lines.

Another (more efficient) possibility, which is investigated here, is to use a 'zebra type' smoother in order to achieve parallelism. With the longer stencils (3), (14) each third line is independent and can be processed at the same time. This means that a parallel zebra type variant is a tri-line zebra smoother, see Figure 3.

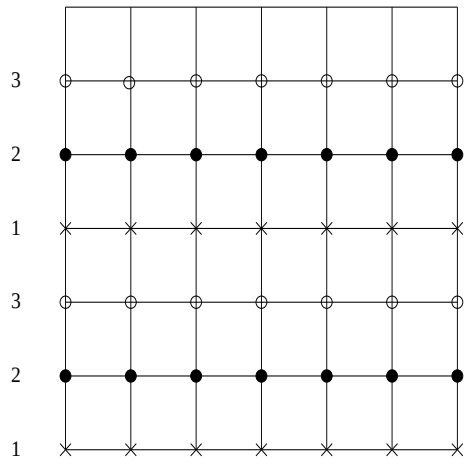

Figure 3: The x-lines that can be processed independently at the same time by a tri-line zebra smoother.

In case of a tri-line smoother the ordering of processing the three lines influences the smoothing behavior. A 1-2-3-processing (see Figure 3) results in other convergence rates than a 1-3-2-processing of lines. In order to obtain a robust smoother for many convection directions, we adopt an ordering of 1-2-3, followed by 1-3-2 as one iteration of the (x-line) tri-line smoother.

Note that the alternating tri-line smoother which we will evaluate, is now as expensive as the alternating symmetric line smoother.

Generalization to 3D. One possible generalization for the smoother presented above to 3D problems is by means of *multiple semicoarsening*. Instead of keeping the standard multigrid sequence, in which then an alternating symmetric line smoother in three directions or for some problems a plane smoother is necessary, one might change the coarsening sequence and include semicoarsening in one or two directions only, as is done in [23]. By using the flexible multiple coarsening grid sequence from [23], it is possible to obtain a 3D robust solution method based on line smoothing.

3 Fourier analysis

3.1 General definitions, remarks

Fourier analysis is used to study the smoothing and convergence properties of the 2D multigrid solution method, like in [2], [20], [24]. It is valid, if we deal with linear (or linearized) operators with constant (or frozen) coefficients, (assume "periodic" boundary conditions) and extend all occurring operators to an infinite grid $G_h := \{\boldsymbol{x} = (k_x h, k_y h) : k_x, k_y \in \mathbb{Z}\}$. On G_h we consider infinite-grid functions, which are linear combinations of the Fourier components $\varphi(\boldsymbol{\theta}, \boldsymbol{x}) = e^{i\boldsymbol{k\theta}} = e^{i(k_x\theta_x + k_y\theta_y)}$ with grid points $\boldsymbol{x} \in G_h$, $\boldsymbol{k} = (k_x, k_y)$ and Fourier frequencies $\boldsymbol{\theta} = (\theta_x, \theta_y) \in \mathbb{R}^2$. Fourier components with $|\boldsymbol{\theta}| := \max\{|\theta_x|, |\theta_y|\} \geq \pi$ are not visible on G_h, since they coincide with components $e^{i\boldsymbol{k}\hat{\boldsymbol{\theta}}}$ where $\hat{\boldsymbol{\theta}} = \boldsymbol{\theta} (\mathrm{mod}\, \pi)$. Therefore, the Fourier space $\boldsymbol{\varepsilon}^h = \mathrm{span}\{e^{i\boldsymbol{k\theta}} : \boldsymbol{\theta} \in \Theta = (-\pi, \pi]^2\}$ contains any infinite grid function on G_h ([20]). The basis functions $e^{i\boldsymbol{k\theta}} \in \boldsymbol{\varepsilon}^h$ are orthogonal with respect to the inner product:

$$(v_h, w_h) := \lim_{m\to\infty} \frac{1}{4m^2} \sum_{|\boldsymbol{k}|\leq m} v_h(\boldsymbol{kh})\, \overline{w_h(\boldsymbol{kh})} \quad \text{with } \boldsymbol{h} = (h, h)\,;\ v_h, w_h \in \boldsymbol{\varepsilon}^h \tag{25}$$

The Fourier space $\boldsymbol{\varepsilon}^h$ can be divided into four-dimensional sub-spaces, *the harmonics* [20] (see Figure 4):

$$\begin{aligned} \boldsymbol{\varepsilon}^h_{\boldsymbol{\theta}} &= \mathrm{span}\{\varphi(\boldsymbol{\theta}^{\alpha_x\alpha_y}, \boldsymbol{x}) = e^{i\boldsymbol{k\theta}^{\alpha_x\alpha_y}}; \alpha_x, \alpha_y \in \{0, 1\}\}, \\ &\text{where } \ \boldsymbol{x} \in G_h;\ \boldsymbol{\theta}^{00} \in \Theta^{00} = (-\pi/2, \pi/2]^2 \\ &\text{and } \ \boldsymbol{\theta}^{\alpha_x\alpha_y} = (\theta_x - \alpha_x \mathrm{sign}(\theta_x)\pi, \theta_y - \alpha_y \mathrm{sign}(\theta_y)\pi) \end{aligned} \tag{26}$$

The discrete solution ϕ_h and the current approximation ϕ_h^m can be represented as linear combinations of the basis functions $e^{i\boldsymbol{k\theta}} \in \boldsymbol{\varepsilon}^h$. This carries over to the error $v^m = \phi^m - \phi_h$ before and $v^{m+1} = \phi^{m+1} - \phi_h$ after a relaxation step or a two-grid cycle.

3.2 Smoothing analysis

In case of Fourier smoothing analysis we look at the influence of a smoothing operator S to the high frequency error components. The multigrid idea consists of the assumption that high frequency error components are smoothed by the relaxation and the low frequency components are reduced by the coarse grid correction. If standard coarsening is selected ($H = 2h$) the components $\varphi(\boldsymbol{\theta}^{00}, x) \in \varepsilon^h$ are also visible on the coarse grid G_H whereas the other components $\varphi(\boldsymbol{\theta}^{\alpha_x\alpha_y}, x)$ with $(\alpha_x, \alpha_y) = (1, 0), (0, 1), (1, 1)$ aliase with the $\varphi(\boldsymbol{\theta}^{00}, x)$ ([20]). This

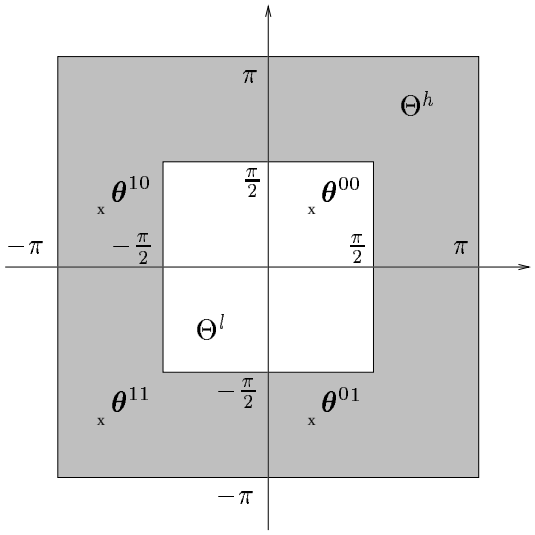

Figure 4: High and low frequency regions of ε^h with four harmonics

observation leads to the distinction between high frequencies $\boldsymbol{\theta} \in \Theta^h := \{\boldsymbol{\theta}^{\alpha_x \alpha_y} : (\alpha_x, \alpha_y) \in \{(1,1),(1,0),(0,1)\}\}$ and low frequencies $\boldsymbol{\theta} \in \Theta^l := \Theta^{00}$ with $\Theta = \Theta^l \cup \Theta^h$ (see Figure 4). The distinction obviously depends on the coarsening strategy.
The relaxation process S applied to an error component $v^m(\boldsymbol{\theta}) = A^m e^{i\boldsymbol{k}\boldsymbol{\theta}}$ results in $v^{m+1}(\boldsymbol{\theta}) = Sv^m(\boldsymbol{\theta})$, which follows from (19), (20) and the identity $L_2\phi_h = f$. Then, (19) and (20) for the forward x-line smoother S^{x_f} lead to:

$$\begin{aligned} S^{x_f} e^{i\boldsymbol{k}\boldsymbol{\theta}} &= [(1-\omega)\tilde{L}^0(\boldsymbol{\theta}) - \omega\tilde{L}^-(\boldsymbol{\theta})] \cdot [\tilde{L}^0(\boldsymbol{\theta}) + \omega\tilde{L}^+(\boldsymbol{\theta})]^{-1} e^{i\boldsymbol{k}\boldsymbol{\theta}} \\ \Longrightarrow \qquad A^{m+1} &= [(1-\omega)\tilde{L}^0 - \omega\tilde{L}^-] \cdot [\tilde{L}^0 + \omega\tilde{L}^+]^{-1} A^m \end{aligned} \tag{27}$$

This means that the error amplitude is reduced by the factor $\mu(\boldsymbol{\theta})$:

$$\mu(\boldsymbol{\theta}) = [(1-\omega)\tilde{L}^0(\boldsymbol{\theta}) - \omega\tilde{L}^-(\boldsymbol{\theta})] \cdot [\tilde{L}^0(\boldsymbol{\theta}) + \omega\tilde{L}^+(\boldsymbol{\theta})]^{-1}, \tag{28}$$

which is called the amplification factor for the frequency $\boldsymbol{\theta}$. $\tilde{L}^0(\boldsymbol{\theta})$, $\tilde{L}^-(\boldsymbol{\theta})$ and $\tilde{L}^+(\boldsymbol{\theta})$ are the Fourier symbols of the corresponding operators.
The definition of the smoothing factor is now given for the x-line smoother by:

$$\mu = \max_{\boldsymbol{\theta} \in \Theta^h} |\mu(\boldsymbol{\theta})| \tag{29}$$

If ν relaxation steps are performed the smoothing factor is given by μ^ν. The definition of the smoothing factor for the symmetric alternating line smoother is straightforward.
As mentioned above Fourier analysis cannot take special boundary conditions into account. It has been observed that sometimes in connection with Dirichlet boundary conditions a more realistic prediction of the smoothing factor is obtained by leaving out the Fourier frequencies with $\theta_x = 0$ or $\theta_y = 0$ (see [24] and the references therein). This leads to a definition of the smoothing factor in case of Dirichlet boundary conditions ([24]).

$$\mu_D = \max_{\boldsymbol{\theta} \in \Theta_D} |\mu(\boldsymbol{\theta})| \quad \text{with} \quad \Theta_D := \Theta^h \setminus \{\boldsymbol{\theta} : \theta_x = 0 \text{ or } \theta_y = 0\} \tag{30}$$

3.3 Two-grid analysis

Analogous to Fourier smoothing analysis we also perform Fourier two-grid analysis, so that the effect of the coarse grid correction and the transfer operators is taken into account theoretically. Error v^m is transformed by a two-grid cycle as follows:

$$v^{m+1} = S^{\nu_2}(I - P_h(L_H)^{-1}R_h L_h)S^{\nu_1}v^m;\ \ v^{m+1} = S^{\nu_2}C_h^H S^{\nu_1}v^m;\ \ v^{m+1} = M_h^H\, v^m \tag{31}$$

The spectral radius $\rho(M_h^H)$ of the linear two-grid operator M_h^H is an indication of the asymptotic speed of the multigrid convergence.
The coarse grid correction operator C_h^H leaves the (4 dimensional) space of harmonics $\boldsymbol{\varepsilon}_{\boldsymbol{\theta}}^h$ (26) with an arbitrary $\boldsymbol{\theta} \in \tilde{\Theta}^{00} = \Theta^{00} \setminus \{\boldsymbol{\theta} :\ \tilde{L}_H(2\boldsymbol{\theta}^{00}) = 0\}$ invariant, $C_h^H\ :\ \boldsymbol{\varepsilon}_{\boldsymbol{\theta}}^h \longrightarrow \boldsymbol{\varepsilon}_{\boldsymbol{\theta}}^h$ (see [20]). This is a consequence of the following relations of the transfer and coarse grid operators:

$$L_h\ :\ \boldsymbol{\varepsilon}_{\boldsymbol{\theta}}^h \longrightarrow \boldsymbol{\varepsilon}_{\boldsymbol{\theta}}^h\,, \quad L_H\ :\ \mathrm{span}\{\varphi(\boldsymbol{\theta},\boldsymbol{x})\} \longrightarrow \mathrm{span}\{\varphi(\boldsymbol{\theta},\boldsymbol{x})\}\,, \tag{32}$$

$$R_h\ :\ \boldsymbol{\varepsilon}_{\boldsymbol{\theta}}^h \longrightarrow \mathrm{span}\{\varphi(\boldsymbol{\theta},\boldsymbol{x})\}\,, \quad P_h\ :\ \mathrm{span}\{\varphi(\boldsymbol{\theta},\boldsymbol{x})\} \longrightarrow \boldsymbol{\varepsilon}_{\boldsymbol{\theta}}^h\,, \quad \text{With: } \boldsymbol{\theta} \in \tilde{\Theta}_{00} \tag{33}$$

The same invariance property is true for each of the above line smoothers (except the tri-line smoother) : $S\ :\ \boldsymbol{\varepsilon}_{\boldsymbol{\theta}}^h \longrightarrow \boldsymbol{\varepsilon}_{\boldsymbol{\theta}}^h$ $(\boldsymbol{\theta} \in \tilde{\Theta}^{00})$. Hence M_h^H is orthogonally equivalent to a block matrix consisting of 4×4 blocks, which will be denoted by $\tilde{M}_h^H(\boldsymbol{\theta}) := M_h^H\,|_{\boldsymbol{\varepsilon}_{\boldsymbol{\theta}}^h}$ $(\boldsymbol{\theta} \in \tilde{\Theta}^{00})$ [20]. We can determine the spectral radius $\rho(M_h^H)$ by calculating the spectral radii of 4×4 matrices:

$$\rho^* = \rho(M_h^H) = \max_{\boldsymbol{\theta}\in\tilde{\Theta}^{00}} \rho(\tilde{M}_h^H(\boldsymbol{\theta})) = \max_{\boldsymbol{\theta}\in\tilde{\Theta}^{00}} \rho(\boldsymbol{\theta}) \tag{34}$$

To obtain the representation of the $4 \times 4-$blocks $\tilde{M}_h^H(\boldsymbol{\theta}) = \tilde{S}^{\nu_2}(I - \tilde{P}_h(\tilde{L}_H)^{-1}\tilde{R}_h\tilde{L}_h)\tilde{S}^{\nu_1}$ the Fourier symbols of the multigrid operators for each harmonic in $\boldsymbol{\varepsilon}_{\boldsymbol{\theta}}^h$ have to be calculated.

$$\tilde{S}^{\nu} = \begin{pmatrix} \mu(\boldsymbol{\theta}^{00}) & & & \\ & \mu(\boldsymbol{\theta}^{10}) & & \\ & & \mu(\boldsymbol{\theta}^{01}) & \\ & & & \mu(\boldsymbol{\theta}^{11}) \end{pmatrix}^{\nu}, \quad \tilde{L}_h = \begin{pmatrix} \tilde{L}_h(\boldsymbol{\theta}^{00}) & & & \\ & \tilde{L}_h(\boldsymbol{\theta}^{10}) & & \\ & & \tilde{L}_h(\boldsymbol{\theta}^{01}) & \\ & & & \tilde{L}_h(\boldsymbol{\theta}^{11}) \end{pmatrix},$$

$$\tilde{R}_h = (\,\tilde{R}_h(\boldsymbol{\theta}^{00}), \tilde{R}_h(\boldsymbol{\theta}^{10}), \tilde{R}_h(\boldsymbol{\theta}^{01}), \tilde{R}_h(\boldsymbol{\theta}^{11})\,)\,, \quad \tilde{P}_h = (\,\tilde{P}_h(\boldsymbol{\theta}^{00}), \tilde{P}_h(\boldsymbol{\theta}^{10}), \tilde{P}_h(\boldsymbol{\theta}^{01}), \tilde{P}_h(\boldsymbol{\theta}^{11})\,)^T\,,$$

$$\tilde{L}_H = \tilde{L}_H(2\boldsymbol{\theta}^{00}) \tag{35}$$

These symbols are calculated, as is done in [20] for the transfer operators.

$$\tilde{L}_h(\boldsymbol{\theta}^{**}) \;=\; \sum_{\mu_x\in J}\sum_{\mu_y\in J} a_{\mu_x\mu_y}^{h(2)} e^{i\theta_x^{**}\mu_x} e^{i\theta_y^{**}\mu_y} \tag{36}$$

$$\tilde{L}_H(2\boldsymbol{\theta}^{00}) \;=\; \sum_{\mu_x\in J}\sum_{\mu_y\in J} a_{\mu_x\mu_y}^{H(2)} e^{i2\theta_x^{00}\mu_x} e^{i2\theta_y^{00}\mu_y} \tag{37}$$

for $a_{\mu_x\mu_y}^{h(2)}$, $a_{\mu_x\mu_y}^{H(2)}$ see (3).
The relation between smoothing and two-grid analysis becomes clear by comparing the definition of the smoothing factor (29) and the definition of ρ^* (34). Smoothing analysis can be regarded as a simplified two-grid analysis, where we replace the *actual* coarse grid operator C_h^H (31) by an *ideal* operator Q_h^H, which annihilates the low frequency error components and leaves the high frequency components unchanged ([20]). With Q_h^H, obviously the coupling between the high

and low frequencies is neglected. It is a projection operator onto the space of high frequencies. Q_h^H can also be represented as a block matrix consisting of 4×4 diagonal blocks $\tilde{Q}_h^H(\boldsymbol{\theta})$. Regarding standard coarsening $\tilde{Q}_h^H(\boldsymbol{\theta})$ looks for all $\theta \in \tilde{\Theta}_{00}$ like:

$$\tilde{Q}_h^H = \begin{pmatrix} 0 & & & \\ & 1 & & \\ & & 1 & \\ & & & 1 \end{pmatrix} \tag{38}$$

Then definition (29) is equivalent to

$$\mu = \max_{\boldsymbol{\theta} \in \tilde{\Theta}^{00}} \rho(\tilde{S}(\boldsymbol{\theta}) \tilde{Q}_h^H(\boldsymbol{\theta})) = \max_{\boldsymbol{\theta} \in \tilde{\Theta}^{00}} \rho(\boldsymbol{\theta}) \tag{39}$$

3.4 Fourier analysis results

The equation on which we perform the Fourier analysis is equation (1) with fixed directions a and b: $a = cos\beta$, $b = sin\beta$. Angle β and parameter ϵ are to be varied. This test problem is also used in [24], where Fourier smoothing analysis is done for many smoothers on the first order upwind discretization of (1). Here, we use κ-scheme discretizations, like (3), and mainly present results of Splitting 1.
We will give results for the symmetric alternating line smoother S, which was also shown to be robust in [24] for the standard upwind discretization. In many cases (for many angles β) the alternating line smoother is already showing very satisfactory convergence, but the symmetric smoother is necessary for robustness over all angles β. Three values of κ are tested: $\kappa = 0$, $\kappa = 1/3$ and $\kappa = -1$. Two cases for ϵ are evaluated: $\epsilon = 10^{-3}$, a relatively easy test case, and $\epsilon = 10^{-6}$, where the convection is really dominating. For underrelaxation parameter ω we also evaluate two values: $\omega = 1$ and $\omega = 0.7$. We show three representative values for angle β for the symmetric alternating line smoother: $\beta = 0^o$, $\beta = 45^o$ and $\beta = 60^o$. Other angles β ($> 90^o$ for example) lead to identical results for the smoother under consideration. We compare Fourier smoothing and two-grid analysis results with numerical calculations for which we take W(0,1)-cycles (meaning no pre-smoothing, 1 post-smoothing iteration). In the numerical calculations Dirichlet boundary conditions are set. The discrepancy in boundary conditions between the analysis (infinite grid "periodic" boundary conditions) and the numerical experiments is reduced by the very fine grid used. In some cases μ_D (30) gives a better prediction than μ. An example, where μ_D (removing the eigenmodes belonging to $\theta_x = 0$ or $\theta_y = 0$) gives a better prediction of the actual convergence is the test case: $\epsilon = 10^{-6}$, $\beta = 0^o$, $\kappa = 0$ and $\omega = 0.7$. Figure 5 shows $\rho(\boldsymbol{\theta})$, $\forall \boldsymbol{\theta} \in \tilde{\Theta}^{00}$ from Fourier smoothing analysis, where $\rho(\boldsymbol{\theta})$ is the maximum of the amplification factors for the corresponding three high frequency harmonics. It can be seen that only for $\theta_x = 0$ a local maximum appears, which is not observed in the multigrid convergence. The convergence with Dirichlet boundary conditions is better predicted by μ_D. In such a case we will mark the value of μ in the tables below with a D.

First we would like to mention that applying standard line-Gauss-Seidel smoothers directly on (3) leads to smoothing factors larger than 1 (and multigrid divergence). This follows from Fourier analysis and it is also observed in the numerical experiments.

An important observation follows from the two-grid Fourier analysis results. We observe, as in the standard upwind case considered in [4], [5], that the characteristic components, which are constant along the characteristics of the advection operator, are not correctly approximated on

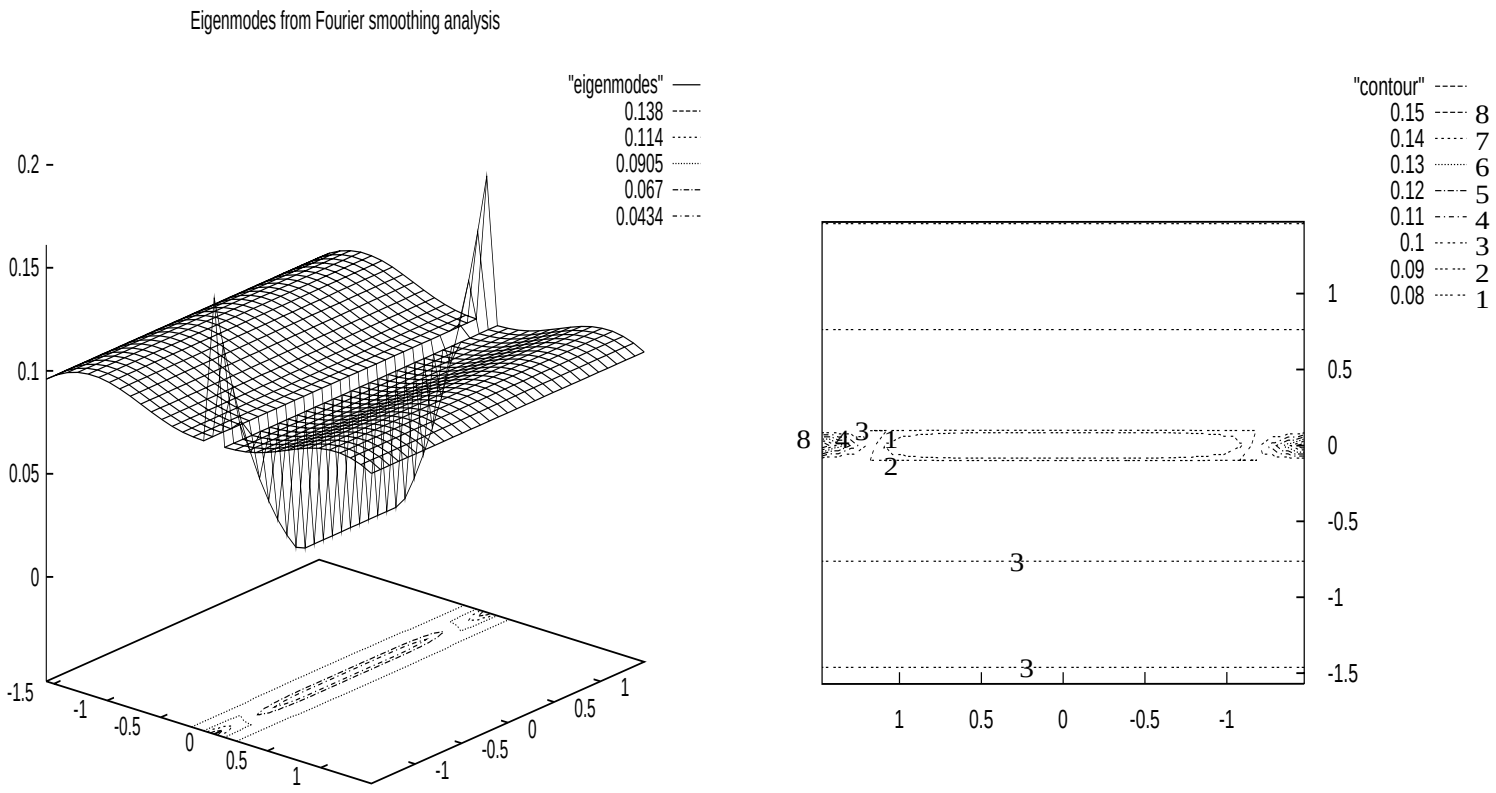

Figure 5: An example of local maximum eigenvalues from Fourier smoothing analysis due to infinite grid "boundary conditions" $h = \frac{1}{64}$ (Splitting 1).

the coarse grid. This phenomenon can be seen from the visualization of the eigenvalues from the two-grid Fourier analysis. For $\beta = 45^o$ these eigenvalues are shown in Figure 6 for $\epsilon = 10^{-3}$, where a maximum radius of 0.45 is observed along the characteristic direction, and in Figure 7 for $\epsilon = 10^{-6}$ where maxima of 0.9 can be seen.
However, we do not observe this bad convergence predicted by the two-grid analysis in our experiments (as in [5]), since we are studying 'inflow/outflow' channel problems and we are using line smoothers. The smoother on the finer grids then also takes care of these problematic error components. (In convection-dominant recirculating flow problems we would use a Krylov acceleration technique ([15]) to improve the multigrid convergence.)
It means, however, that we cannot use ρ^* (34) as a reliable prediction of the multigrid convergence. Since the spectrum is continuous, as can be seen in Figures 6 and 7, it is not possible to remove some modes in order to estimate ρ^*. Therefore, we will give for ρ^* in the tables below an 'intuitive estimation' of the maximum of $\rho(M_h^H)$ away from the characteristic direction. We look for a local maximum at the boundary of the frequency domain, not in the characteristic direction. It will be seen that this estimation is often a good prediction for a multigrid convergence factor. A fine equidistant grid with mesh size $h = 1/256$ is chosen in $\Omega = (0,1)^2$.

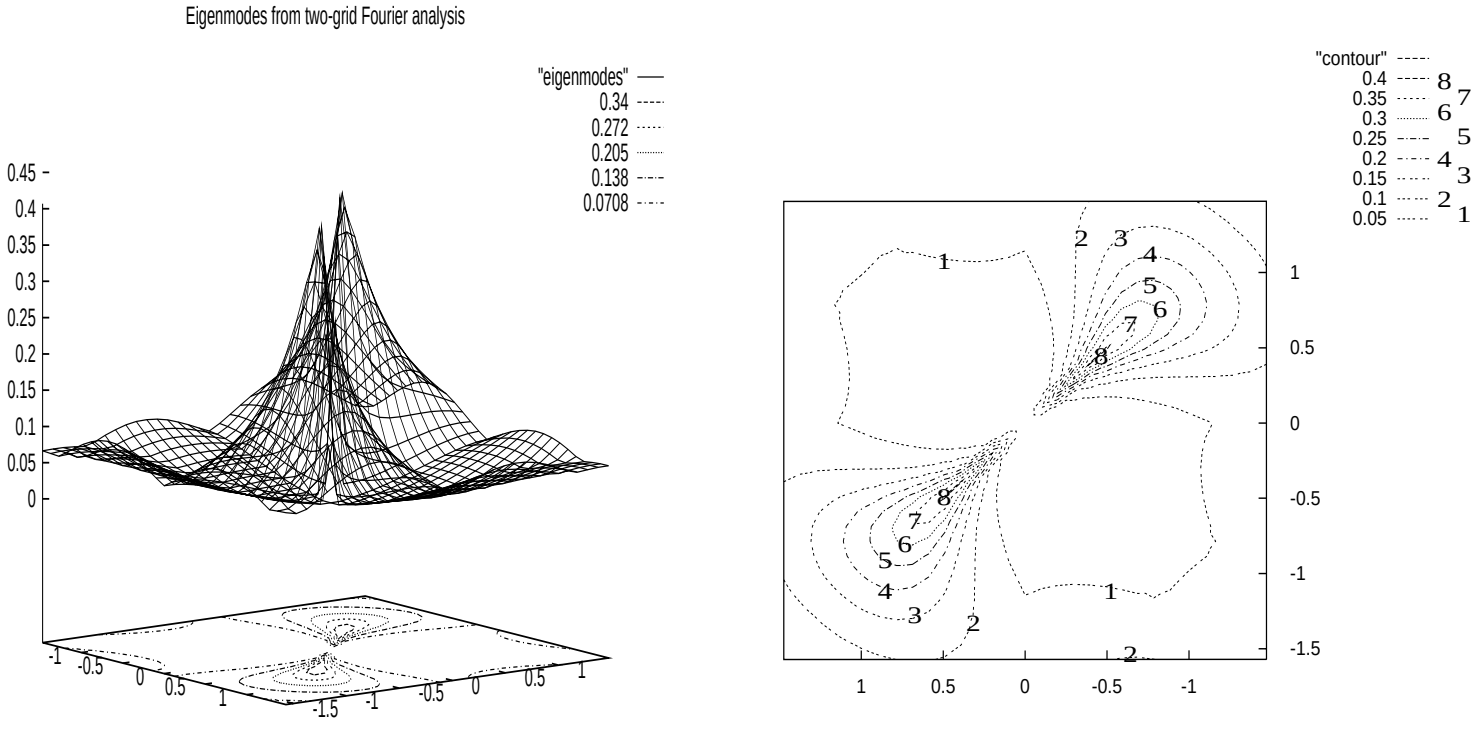

Figure 6: Large error components corresponding to low frequency harmonics along the characteristic components of the advection operator $(a,b)^T = (\frac{1}{\sqrt{2}}, \frac{1}{\sqrt{2}})^T$ for $\epsilon = 10^{-3}$, following from two-grid Fourier analysis for Splitting 1, $h = \frac{1}{64}$.

The results from Fourier analysis are compared for the test cases mentioned with the multigrid convergence in Tables I and II. In Table I results are presented for $\epsilon = 10^{-3}$, in Table II for $\epsilon = 10^{-6}$. The results from these tables are obtained with the alternating symmetric KAPPA smoother from Splitting 1. With Splitting 2 results with $\kappa = 0$ are identical, with $\kappa = 1/3$ are similar, but the results with $\kappa = -1$ are not robust: For angles $\beta = 20^o$ and $\beta = 70^o$ smoothing (and convergence) factors much larger than 1 are always obtained. An average reduction factor over 100 iterations is taken as multigrid convergence rate.
Also results from Fourier smoothing analysis with *pointwise* KAPPA smoothers, based on Splitting 1, show a very satisfactory smoothing behavior: Pointwise smoothers in the flow direction will lead to very fast optimized multigrid methods for specific problems, and four-direction point smoothers, where each step starts in a different corner of a rectangular grid, will be robust for the convection-diffusion problem with respect to all angles β.

Tables I and II show that the smoothing factor μ (μ_D) and the (intuitive) two-grid factor ρ^* give a very good indication of the actual asymptotic multigrid convergence on the fine grid. The dependence of the convergence on different values of κ, ϵ or ω is very well predicted by Fourier analysis. Furthermore, the convergence of the W(0,1)-cycle is very satisfactory. For $\epsilon = 10^{-3}$

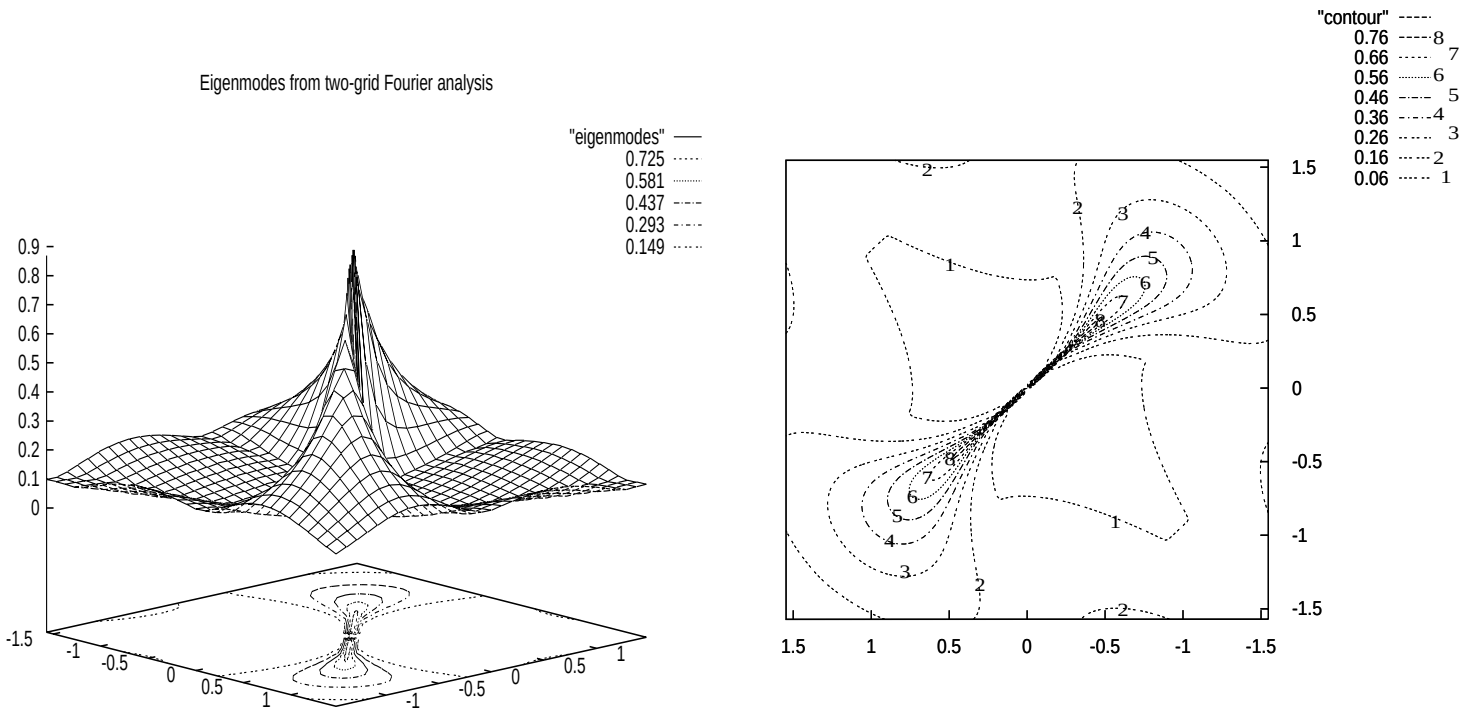

Figure 7: Large error components corresponding to low frequency harmonics along the characteristic components of the advection operator $(a,b)^T = (\frac{1}{\sqrt{2}}, \frac{1}{\sqrt{2}})^T$ for $\epsilon = 10^{-6}$, following from two-grid Fourier analysis for Splitting 1, $h = \frac{1}{64}$.

all convergence factors are smaller than 0.3, for $\kappa = -1$ and $\kappa = 0$ and $\omega = 1$ even smaller than 0.1. Also for the difficult test case $\epsilon = 10^{-6}$ the convergence rates are small, especially for $\kappa = -1$. It appears that $\omega = 1$ (no underrelaxation) is best for the test cases considered with the alternating symmetric KAPPA smoother.

Remark: Note that for the convection-dominated scalar problems the single grid line solvers (using the smoother as a solver) also give a very satisfactory convergence. For scalar problems with regions of dominating convection and diffusion, of course, multigrid is again necessary for good convergence. We will show the benefits of multigrid (compared to single grid) by analyzing the convergence of problems with a nonconstant convection direction in the the next section.

Remark: The spectral radius ρ is, of course, a measure of the asymptotic convergence of a solution method. In case of convection-dominated problems (resulting in nonsymmetric matrices) it might take a long time before asymptoticity is observed. As an alternative it makes sense to consider norms of the iteration matrix, as in [20], or half-space FMG estimates as a practical measure of convergence, as is done in [3]. We again refer to the problems in the next section to observe the actual convergence for some representative test problems.

$\epsilon = 10^{-3}$

β		$\kappa = -1$		$\kappa = 0$		$\kappa = \frac{1}{3}$	
		$\omega = 0.7$	$\omega = 1.0$	$\omega = 0.7$	$\omega = 1.0$	$\omega = 0.7$	$\omega = 1.0$
0	μ	0.117	0.050	0.101	0.048	0.123	0.050
	ρ^*	0.124	0.051	0.113	0.059	0.140	0.060
	$W(0,1)$	0.122	0.055	0.110	0.041	0.120	0.053
45	μ	0.128	0.025	0.155	0.043	0.170	0.056
	ρ^*	0.139	0.028	0.162	0.10	0.173	0.047
	$W(0,1)$	0.093	0.060	0.220	0.093	0.187	0.050
60	μ	0.156	0.033	0.161	0.046	0.166	0.054
	ρ^*	0.194	0.027	0.185	0.058	0.164	0.046
	$W(0,1)$	0.183	0.053	0.200	0.094	0.168	0.058

Table I: A comparison of Fourier analysis results with multigrid convergence for the convection-diffusion equation for $\epsilon = 10^{-3}$ (Splitting 1), $h = \frac{1}{256}$.

We do not perform Fourier analysis for the alternating tri-line smoother from Section 2.2, but we apply this smoother to the same problems, that are presented in the Tables I and II. In Table III we show the multigrid convergence for the alternating tri-line smoother with $\omega = 0.7$ for $\kappa = 0$, $\epsilon = 10^{-6}$ for different numbers of pre- and post-smoothing iterations. The first column of Table III can be compared to the results in Table II. In Table III we also evaluate $\beta = 225^o$, since for this smoother the results obtained are not angle-independent, as mentioned in Section 2.2. It is found that for all angles satisfactory convergence results are obtained also with the alternating tri-line smoother. From Table III it can be seen that the convergence obtained with the tri-line smoother is a bit worse than the convergence with the symmetric alternating line smoother in Table II (which is to be expected). Furthermore, it can be seen that the multigrid convergence strongly improves, when more smoothing iterations are performed. The addition of one smoothing iteration has more than doubled the multigrid convergence speed in the cases considered.
We would like to conclude with two pictures of the eigenvalue spectra of multigrid iteration matrices for a problem investigated in this section ($\epsilon = 10^{-6}$, $\beta = 0^o$, $\kappa = 0$) on a 32×32 grid. The first picture, Figure 8 shows the spectrum obtained with the W(0,1)-cycle and the alternating tri-line KAPPA smoother with $\omega = 0.7$. One sees the clustering around the origin and a spectral radius of 0.1 on this relatively coarse grid.
The second picture, Figure 9, is the spectrum found for the same problem with the classical defect correction iteration. The first order discretization, which is inside the defect correction technique, is solved with a high accuracy by a multigrid solver. In Figure 9 a completely different spectrum is found without a clustering around the origin and a spectral radius of 0.5. The difference in spectra of Figures 8 and 9 is remarkable.

4 Numerical results

The problems in this section are solved with the multigrid methods described in Section 2.2. In some of the experiments we compare the convergence with the defect correction convergence. The initial iterand ϕ_h^0 is mostly obtained with the full multigrid method (FMG). We fix the

$\epsilon = 10^{-6}$

β		$\kappa = -1$		$\kappa = 0$		$\kappa = \frac{1}{3}$	
		$\omega = 0.7$	$\omega = 1.0$	$\omega = 0.7$	$\omega = 1.0$	$\omega = 0.7$	$\omega = 1.0$
0	μ	0.283	0.001^D	0.104^D	0.079	0.152^D	0.175
	ρ^*	0.283	0.004	0.104	0.080	0.153	0.175
	$W(0,1)$	0.277	0.001	0.100	0.080	0.145	0.176
45	μ	0.226	0.057	0.365	0.177	0.432	0.289
	ρ^*	0.236	0.053	0.360	0.165	0.452	0.308
	$W(0,1)$	0.320	0.050	0.420	0.180	0.407	0.277
60	μ	0.347	0.107	0.473	0.220	0.567	0.326
	ρ^*	0.334	0.083	0.455	0.152	0.560	0.327
	$W(0,1)$	0.356	0.050	0.360	0.140	0.452	0.330

Table II: A comparison of Fourier analysis results with multigrid convergence for the convection-diffusion equation for $\epsilon = 10^{-6}$ (Splitting 1), $h = \frac{1}{256}$.

β	$W(0,1)$	$W(0,2)$	$W(1,2)$
0	0.18	0.036	0.008
45	0.58	0.22	0.055
60	0.57	0.16	0.048
225	0.49	0.13	0.056

Table III: Multigrid convergence for the alternating tri-line smoother for the convection-diffusion problem with $\kappa = 0$, $\epsilon = 10^{-6}$.

underrelaxation parameter ω for the different smoothers that are evaluated here: The symmetric alternating KAPPA smoother based on Splitting 1 is always used without damping ($\omega = 1$), the symmetric alternating KAPPA smoother based on Splitting 2 uses underrelaxation $\omega = 0.7$, as both alternating tri-line KAPPA smoothers. These values showed the best multigrid performance for the problems in the previous section.

4.1 Convection-diffusion with analytical solution

For the first example we consider the convection-diffusion equation (1) with the convective terms coming from the Smith-Hutton problem ([17]):

$$-\epsilon\Delta\phi + 2y(1-x^2)\phi_x - 2x(1-y^2)\phi_y = f \tag{40}$$

where ϵ is a small positive number ($\epsilon = 10^{-6}$). This problem is interesting, since many angles are encountered by the definition of $a(x,y)$ and $b(x,y)$. This means that (40) is a good indication for the robustness of a solver. The domain is chosen as follows:

$$\Omega = \{(x,y); -1 \le x \le 1, 0 \le y \le 1\} \tag{41}$$

In the first example right-hand side f and the Dirichlet boundary conditions are chosen such

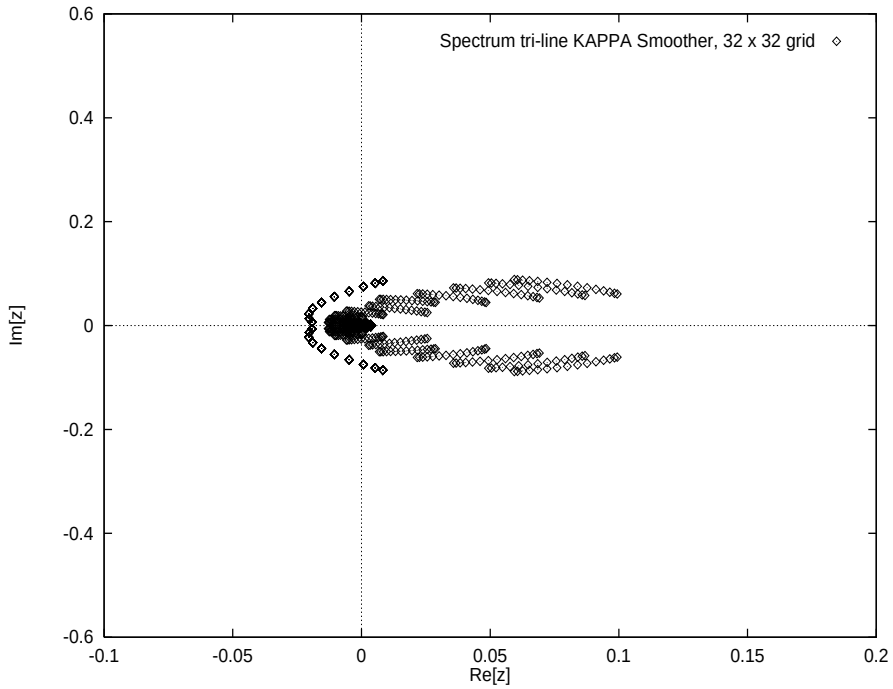

Figure 8: Spectrum of the multigrid iteration matrix with the alternating tri-line KAPPA smoother, $\epsilon = 10^{-6}, \beta = 0^o, \kappa = 0$, $h = \frac{1}{32}$.

that a smooth analytical solution results:

$$\phi = x^4 + y^4 \tag{42}$$

A limiter is not necessary for this problem, and we can compare the accuracy of the κ-schemes. The multigrid convergence is shown with the symmetric alternating KAPPA smoother ($\omega = 1$) and the tri-line alternating zebra KAPPA smoother ($\omega = 0.7$) from Splitting 1 on a fine grid $(h_x, h_y)^T = (2/256, 1/128)^T$. A multigrid V-cycle processing 7 levels is used with 2 pre- and 1 post-smoothing iterations. We present results for $\kappa = 0$ and $\kappa = -1$. Furthermore, in the Figures 10a and 10b the convergence of the classical defect correction iteration is presented.
The multigrid convergence with both KAPPA smoothers is very satisfactory: The best smoother converges within 5 multigrid iterations. The symmetric alternating line smoother is twice as fast as the tri-line smoother for this problem. For this smooth problem the improvement in the higher order residual reduction compared to the classical approaches for $\kappa = 0$ is very satisfactory. It can be seen that the convergence of defect correction stops for the discretization with $\kappa = -1$. However, the difference in L_2-norm between the numerical solution and the analytical solution for the defect correction iteration and the KAPPA smoothers is almost the same. Table IV presents the number of iterations and the wall-clock time needed to reduce the initial residual by 6 orders of magnitude. This can be seen as an indication for the convergence in the initial stage of residual reduction, which is not indicated by a spectral radius. The wall-clock times are relatively large, since the implementation is not done most efficiently. The emphasize has been laid upon storage reduction, not on obtaining the best timings. Operator elements are re-calculated on every grid, although the operator and the discretization are linear. It can be seen that with the symmetric alternating line smoother a very fast and level independent convergence

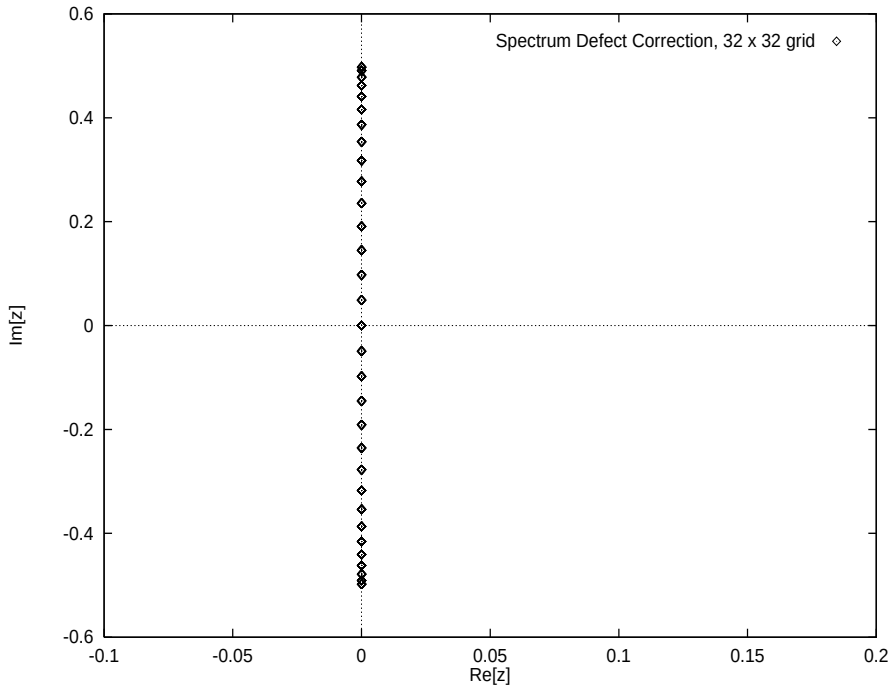

Figure 9: Spectrum of the defect correction iteration matrix with a multigrid solver for the inner iteration, $\epsilon = 10^{-6}, \beta = 0^o, \kappa = 0$, $h = \frac{1}{32}$.

is obtained for this test problem. (For these grid sizes, also the single grid solver is still very fast and in wall-clock time comparable to the multigrid convergence.) The number of iterations grows somewhat for increasing grid sizes with the tri-line smoother. In Table V, we can observe the accuracy of the κ-schemes by comparing the numerical to the analytical solution on fine grid sizes. We present the difference in L_∞-norm and L_2-norm and an estimation of the discretization order p. It can be seen from Table V that second order accuracy is obtained for both κ-values. Further, it should be mentioned that the second order accuracy is already reached after one FMG cycle.

grid	alt. symmetric smoother		alt. tri-line smoother	
	$\kappa = 0$	$\kappa = -1$	$\kappa = 0$	$\kappa = -1$
64×32	3 (1.1)	3 (1.1)	5 (2.6)	6 (3.2)
128×64	3 (6.4)	3 (6.4)	6 (11.8)	8 (15.0)
256×128	3 (24.9)	4 (32.8)	7 (54.5)	9 (70)
512×256	3 (102.5)	4 (136)	9 (286)	10 (320)

Table IV: Level independent convergence and corresponding wall-clock time in seconds (in brackets) with two κ-schemes for a convection-diffusion problem with an analytical solution.

κ-scheme	grid	$\|\|\phi\|\|_\infty$	p_∞	$\|\|\phi\|\|_2$	p_2
$\kappa = 0$	64×32	5.7486×10^{-3}	-	1.5095×10^{-3}	-
	128×64	1.5041×10^{-3}	1.93	3.1204×10^{-4}	2.27
	256×128	4.0707×10^{-4}	1.88	7.1283×10^{-5}	2.13
$\kappa = -1$	64×32	9.1171×10^{-3}	-	2.8992×10^{-3}	-
	128×64	2.4513×10^{-3}	1.89	6.3281×10^{-4}	2.19
	256×128	6.5561×10^{-4}	1.90	1.4332×10^{-4}	2.14

Table V: The accuracy achieved with the κ-scheme for a convection-diffusion problem with an analytical solution.

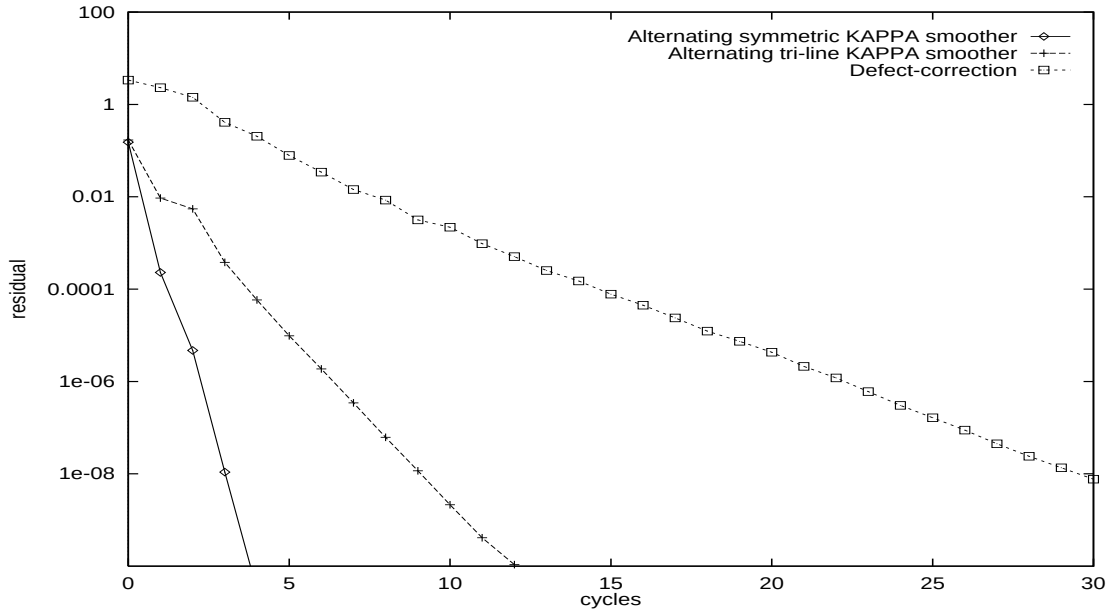

(a)

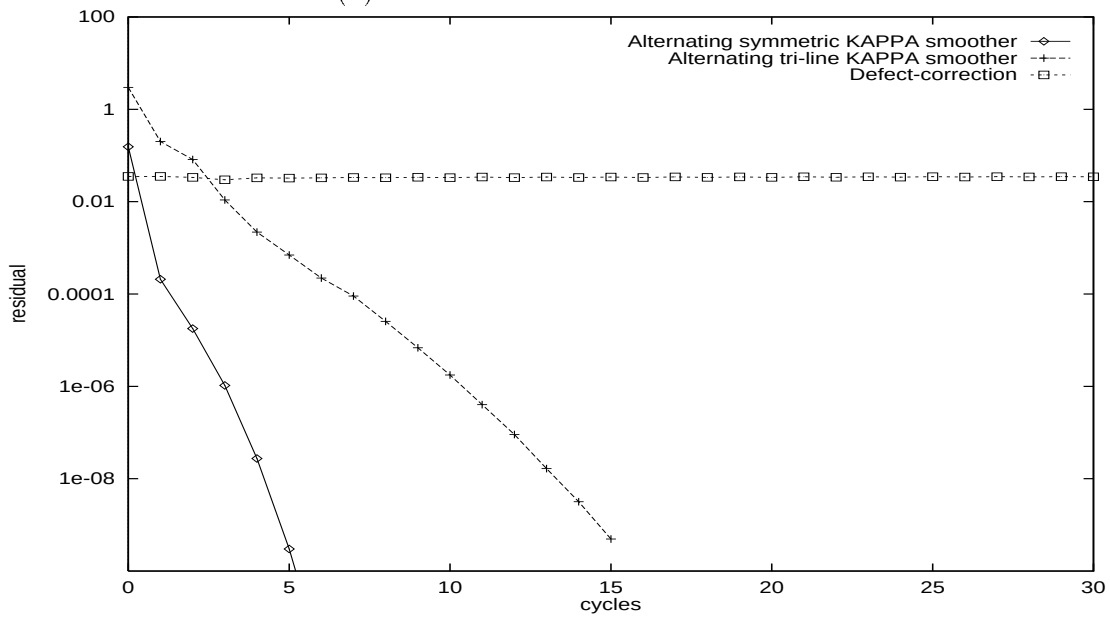

(b)

Figure 10: The multigrid convergence of three approaches for the Smith-Hutton problem with analytical solution with (a): $\kappa = 0$ and (b): $\kappa = -1$, 256×128-grid.

4.2 Convection-diffusion with discontinuous boundary condition

The second problem is also based on equation (40), the Smith-Hutton problem with $f = 0$ on domain (41). The difficulty comes from the boundary condition which looks like:

$$\begin{aligned} \phi|_{\partial\Omega} &= 2 \text{ on } \partial\Omega : -\frac{1}{2} \leq x \leq 0.5,\ y = 0 \\ \phi|_{\partial\Omega} &= 0 \text{ elsewhere} \end{aligned} \tag{43}$$

The solution contains a step-like discontinuity which moves along the characteristics of the advection operator. Limiters are really necessary to assure an accurate solution. Figure 11 presents the solution. Instead of investigating the sharpness of the discontinuity profile with different limiters, as is done in many other papers like [17], or for other problems for example in [16] or [14], we concentrate on the convergence of the multigrid solution methods. Again the

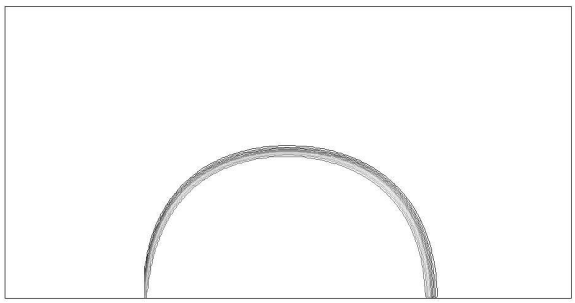

Figure 11: The solution of the Smith-Hutton problem with discontinuous boundary condition.

multigrid convergence on the fine grid $(h_x, h_y)^T = (2/256, 1/128)^T$ is investigated with V(2,1)-cycles. Here, we present results obtained with the alternating tri-line smoothers, and evaluate the difference in convergence between the smoothers based on Splitting 1 and Splitting 2 for the limited discretizations. Often for example for several systems of equations it is more expensive to compute $L_2\phi$ than $L_1\phi$ even on coarse grids. Therefore, we test whether for this problem with a step discontinuity solution it makes sense to use a discretization based on L_1 on the coarse grids as well. Figure 12 presents the multigrid convergence results with two limiters from the first class of limiters, the ISNAS limiter (9), see Figure 12a, and the van Leer limiter (8), see Figure 12b, and one limiter from the second class of limiters, the SMART limiter (11), see Figure 12c.

Very satisfactory convergence is observed from the Figures 12a and 12b. Especially the 'engineering accuracy' $|(f - L_2\phi^m)|/|(f - L_2\phi^0)| \leq 10^{-6}$ is reached very fast. Furthermore, it is observed that the difference in convergence with L_1 as the coarse grid discretization is not significant. Also we see that smoothers based on both Splitting 1 and Splitting 2 result in acceptable convergence on this fine grid. These results were found to be representative for other limiters from this first class.

In Figure 12c it is shown that for the $2R$-based limiter SMART multigrid algorithms based on Splitting 2 have convergence problems. The smoothers based on Splitting 1 do not show a regular convergence, but the residual is reduced by 6 orders of magnitude after 30 iterations, which is satisfactory. Further, we show for the ISNAS and the van Leer limiter, that for these scalar convection-dominated problems, it is not so easy to beat the single grid solver (using the smoother as a solver). Actually, only on very fine grids the benefits of multigrid (tri-line

smoother, Splitting 2, full second order formulation) are clearly observed. The fastest multigrid solver is here the V(0,1)-cycle in case of the van Leer limiter, which is not level independent in convergence. The number of iterations of the single grid solver on the 256×128 grid with the van Leer limiter until engineering accuracy is reached is 39, taking 110 seconds. The V(0,1)-cycle took 26 iterations and 96.5 seconds. On a 4 times finer grid the single grid solver takes 72 iterations in 831 seconds, while 42 iterations in 645 seconds are needed by a V(0,1)-cycle (without nested iteration). For the ISNAS limiter, we find that the single grid solver takes 44 iterations and 126 seconds; the V(0,1)-cycle 30 iterations and 110 seconds. On the 512×256 grid the difference is more pronounced: 76 iterations in 887 seconds for the single grid solution method and 29 iterations in 758 seconds for the V(1,1)-cycle, which appeared to be fasted for the ISNAS limiter on this fine grid. On coarser grids the solution times for single and multigrid solvers based on this alternating symmetric line solver are more or less identical.

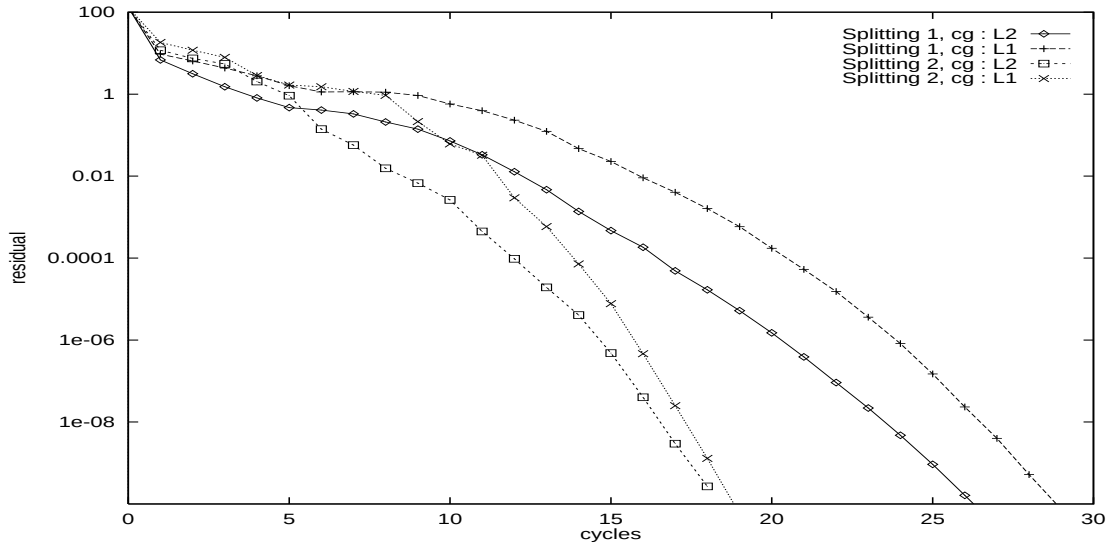

(a)

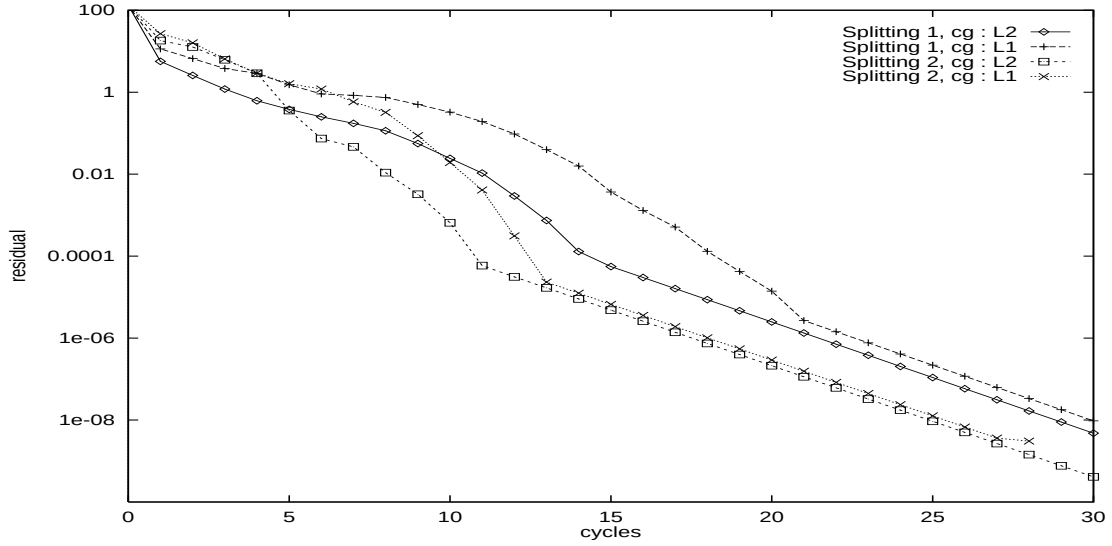

(b)

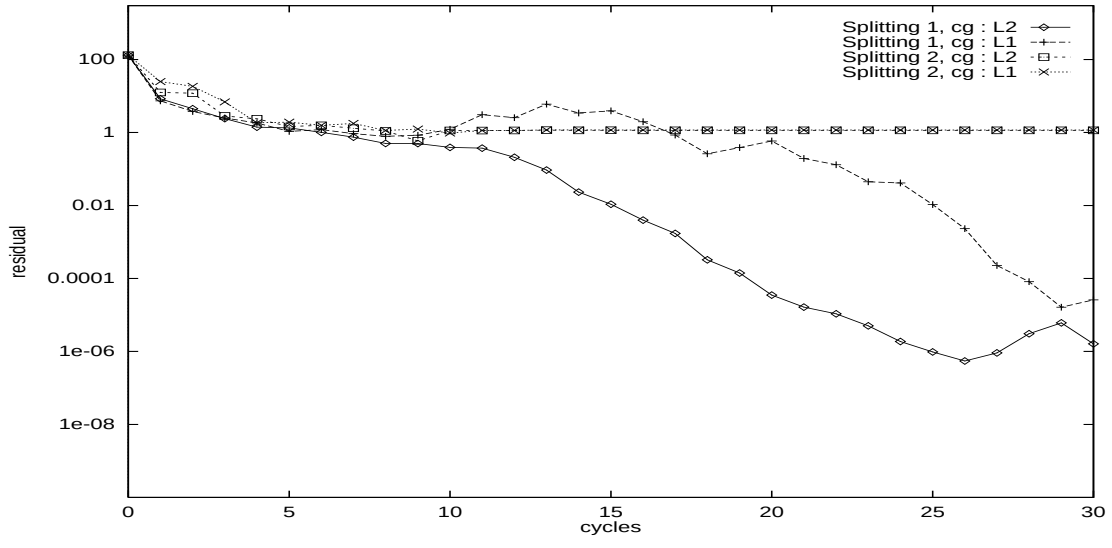

(c)

Figure 12: The multigrid convergence with the two splittings for the alternating tri-line smoother, Smith-Hutton problem with discontinuous boundary condition, 256×128 grid. (a) Convergence with the ISNAS limiter (9), (b) with the van Leer limiter (8), (c) with the SMART limiter (11).

4.3 Nonlinear problem with a shock

We consider the following nonlinear convection-dominated conservation law:

$$-\epsilon\Delta\phi + \left(\frac{\phi^2}{2}\right)_x + \phi_y = 0. \tag{44}$$

Again we put $\epsilon = 10^{-6}$ and boundary conditions are given along the x-axis by

$$\phi_0 = \frac{1}{2}(sin(\pi x) + 1) \tag{45}$$

This scalar nonlinear problem is also studied and described in detail in [16]. The computational domain is: $\Omega = \{(x, y); 0 \leq x \leq 3, 0 \leq y \leq 2\}$.
The exact solution is constant along the characteristic lines $(\phi, 1)^T$. For every point (x, y) we can find a boundary point $(x_0, 0)$ where the characteristic line goes through by solving the implicit equation: $x_0 = x - \phi_0(x_0)y$. The solution becomes unique if we discretize by a conservative finite volume discretization, i.e. if we satisfy the entropy condition for hyperbolic conservation laws ([16]). The solution shown in Figure 13 will contain a shock wave along the line $y = 2x - 2$. Limiters are necessary for an accurate solution of this problem.

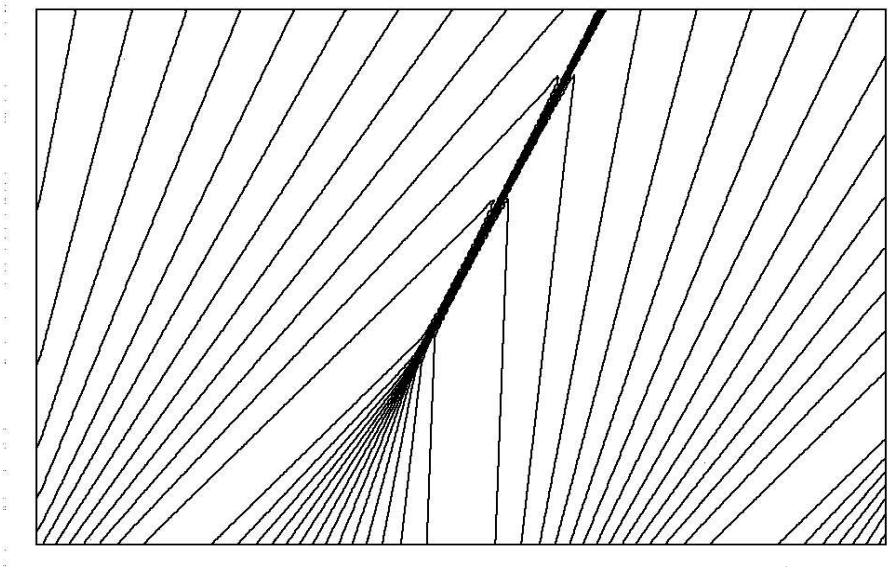

Figure 13: Characteristic lines and shock wave for the nonlinear problem.

We will investigate the multigrid convergence for the ISNAS and van Leer limiters from class 1 and for the SMART limiter from class 2. Again a very fine grid is chosen to see asymptotic convergence: $(h_x, h_y)^T = (3/384, 2/256)^T$. The multigrid V(2,1)-cycle is performed on 8 multigrid levels. We choose L_2 as the coarse grid discretization in this test, and compare the alternating symmetric KAPPA smoother from Splitting 1 with Splitting 2 and with the alternating tri-line smoothers. (The underrelaxation parameters were given at the beginning of this section.) Figure 14a presents the convergence results for the discretization with the ISNAS limiter, Figure 14b with the van Leer limiter and Figure 14c with the SMART limiter.
A similar convergence as for the previous Smith-Hutton problem can be seen in the Figures 14. Splitting 2 gives a somewhat better convergence for the limiters from class 1 than Splitting 1.

Furthermore, the behavior of the symmetric and the tri-line smoother is similar to the previous problems. In the worst case 10 extra multigrid iterations are necessary for the parallel variant.

For the SMART limiter again the convergence stops with smoothers based on Splitting 2, whereas better convergence is obtained with the smoother from Splitting 1. The difference in convergence between discretizations based on limiters from class 1 and class 2 is remarkable. The difference in accuracy with different limiters on these fine grids is relatively small. The convergence until engineering accuracy is reached on several grids is presented in Table VI. Although the convergence is not fully level independent, it is considered very satisfactory, es-

grid	alt. symmetric smoother		alt. tri-line smoother	
	v. Leer	ISNAS	v. Leer	ISNAS
96×64	12	10	12	10
192×128	14	14	16	15
384×256	16	21	22	26

Table VI: Convergence for the nonlinear problem with two limiters on different grids, Splitting 2, full second order formulation.

pecially for the symmetric alternating line smoother. Finally, the single grid solver behaves for this convection-dominated nonlinear scalar problem similarly as for the Smith-Hutton problem from the previous subsection.

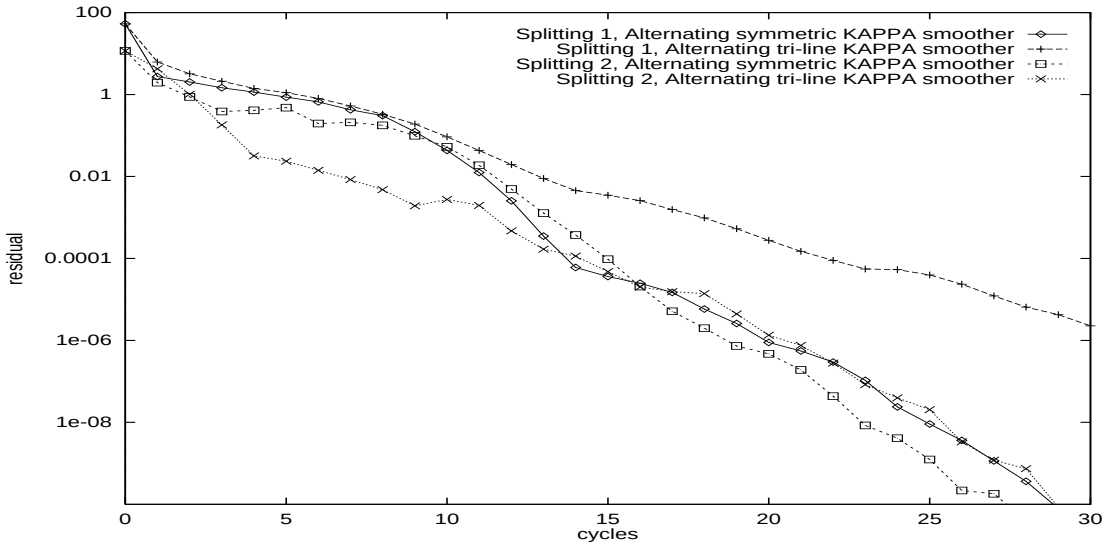

(a)

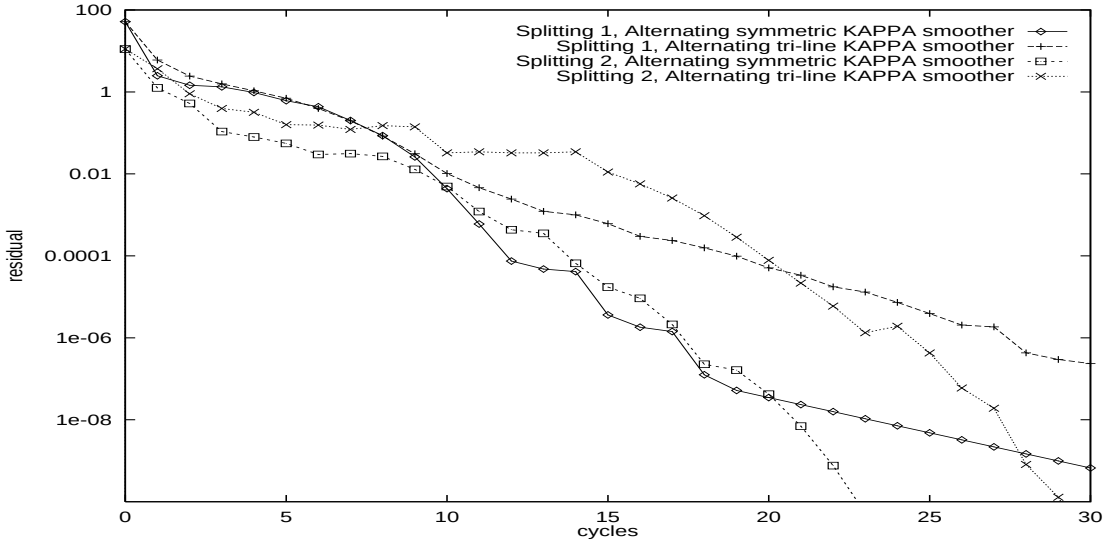

(b)

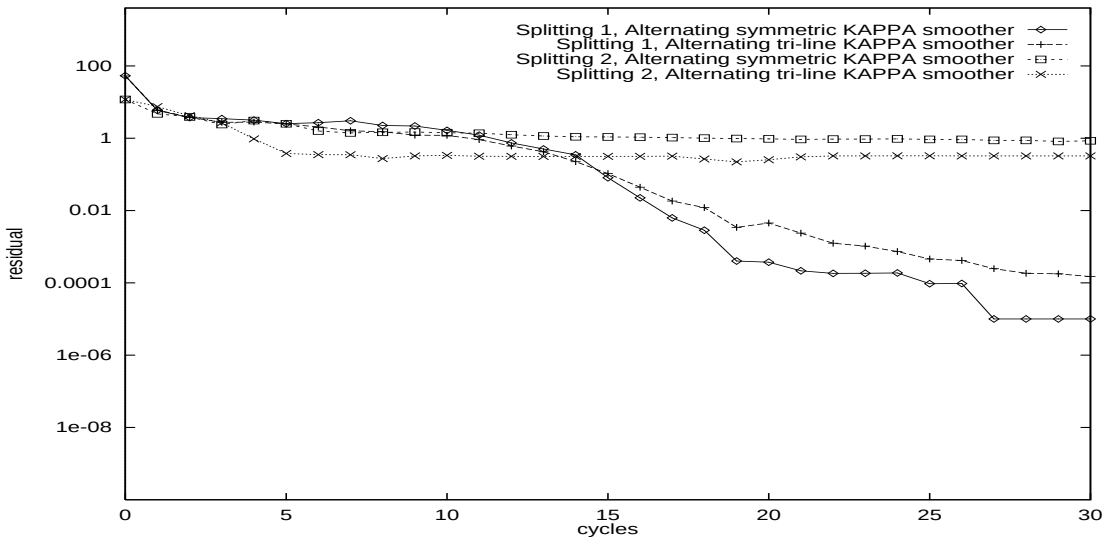

(c)

Figure 14: The multigrid convergence for the nonlinear problem containing a shock with the two splittings for the alternating symmetric and the alternating tri-line smoother, 384×256 grid. (a) Convergence with the ISNAS limiter (9), (b) with the van Leer limiter (8), (c) with the SMART limiter (11).

4.4 An incompressible Navier-Stokes driven cavity example

Next, an incompressible flow example is treated. The 2D steady incompressible Navier-Stokes equations are written as a system of equations as follows,

$$\frac{\partial \mathbf{f}}{\partial x} + \frac{\partial \mathbf{g}}{\partial y} = \frac{\partial \mathbf{f_v}}{\partial x} + \frac{\partial \mathbf{g_v}}{\partial y} \tag{46}$$

where $\mathbf{f}$ and $\mathbf{g}$ are the components of the convective flux vector, and $\mathbf{f_v}$ and $\mathbf{g_v}$ are the viscous fluxes:

$$\mathbf{f} = \begin{bmatrix} u^2+p \\ uv \\ c^2 u \end{bmatrix} \quad , \quad \mathbf{g} = \begin{bmatrix} uv \\ v^2+p \\ c^2 v \end{bmatrix} \quad , \quad \mathbf{f_v} = \begin{bmatrix} \frac{1}{Re}\partial u/\partial x \\ \frac{1}{Re}\partial v/\partial x \\ 0 \end{bmatrix} \quad , \quad \mathbf{g_v} = \begin{bmatrix} \frac{1}{Re}\partial u/\partial y \\ \frac{1}{Re}\partial v/\partial y \\ 0 \end{bmatrix}$$

Here u and v are Cartesian velocity unknowns, p is pressure, c is a constant reference velocity and Re is the Reynolds number defined as: $Re = \overline{U}.L/\nu$, with $\overline{U}$ a characteristic velocity, L a characteristic length and ν the kinematic viscosity.
We solve the incompressible Navier-Stokes equation in the primitive variables. The 2D vertex-centered discretization of (46) (on a collocated grid) is Dick's flux difference splitting, presented in [6]. The resulting stencil from a first order discretization looks as follows:

$$\begin{bmatrix} \begin{matrix} -\frac{1}{Re}\Delta + 2u\partial_x + v\partial_y - \\ \frac{h}{2}(|v|\partial_{yy} + \frac{2u^2+c^2}{\sqrt{u^2+c^2}}\partial_{xx}) \end{matrix} & \begin{matrix} u\partial_y - \\ \frac{huv}{2(v^2+c^2)}(2\sqrt{v^2+c^2} - |v|)\partial_{yy} \end{matrix} & \begin{matrix} \partial_x - \\ \frac{hu}{2}(\frac{1}{\sqrt{u^2+c^2}}\partial_{xx} + \frac{\sqrt{v^2+c^2}-|v|}{v^2+c^2}\partial_{yy}) \end{matrix} \\ \begin{matrix} v\partial_x - \\ \frac{huv}{2(u^2+c^2)}(2\sqrt{u^2+c^2} - |u|)\partial_{xx} \end{matrix} & \begin{matrix} -\frac{1}{Re}\Delta + u\partial_x + 2v\partial_y - \\ \frac{h}{2}(|u|\partial_{xx} + \frac{2v^2+c^2}{\sqrt{v^2+c^2}}\partial_{yy}) \end{matrix} & \begin{matrix} \partial_y - \\ \frac{hv}{2}(\frac{1}{\sqrt{v^2+c^2}}\partial_{yy} + \frac{\sqrt{u^2+c^2}-|u|}{u^2+c^2}\partial_{xx}) \end{matrix} \\ \begin{matrix} c^2\partial_x - \\ \frac{hc^2 u}{2\sqrt{u^2+c^2}}\partial_{xx} \end{matrix} & \begin{matrix} c^2\partial_y - \\ \frac{hc^2 v}{2\sqrt{v^2+c^2}}\partial_{yy} \end{matrix} & \frac{hc^2}{2}(\frac{1}{\sqrt{u^2+c^2}}\partial_{xx} + \frac{1}{\sqrt{v^2+c^2}}\partial_{yy}) \end{bmatrix} \tag{47}$$

where the three entries are for $(u, v, p)^T$, respectively. Here ∂ represents a central discretization, the terms ∂_{xx} and ∂_{yy} are artificial dissipation terms.
Second order accuracy is achieved by replacing the first order convective discretization, which is implicitly in (47), by (3) with $\kappa = 0$. Then, the resulting stencil is similar to (47) with higher order artificial dissipation terms. For incompressible Navier-Stokes equations it is not necessary to implement a limiter. For many different (2D and 3D) problems at low and high Reynolds numbers oscillations (for example in the pressure distribution, as they occur near discontinuities for compressible flow problems) did not appear.
A well-known 2D test case is the lid-driven cavity flow in a unit square. Although this problem is a rotating flow problem, for which standard multigrid schemes might have convergence difficulties, we do not observe these difficulties, since a moderate Reynolds number ($Re = 1000$) is evaluated here. We solve this problem on a 192^2 grid with stretching. With the 192^2 stretched grid the centerline velocity profiles agree very well with reference results from [9]. (A very similar profile is already obtained by solving the problem on a 64×64 equidistant grid.) Figure 15 presents the u-velocity profile in the vertical centerline of the cavity.
The multigrid FAS scheme used for solving this problem is the same as for the scalar problems. The KAPPA smoother is now a *coupled collective* symmetric alternating line smoother, and a

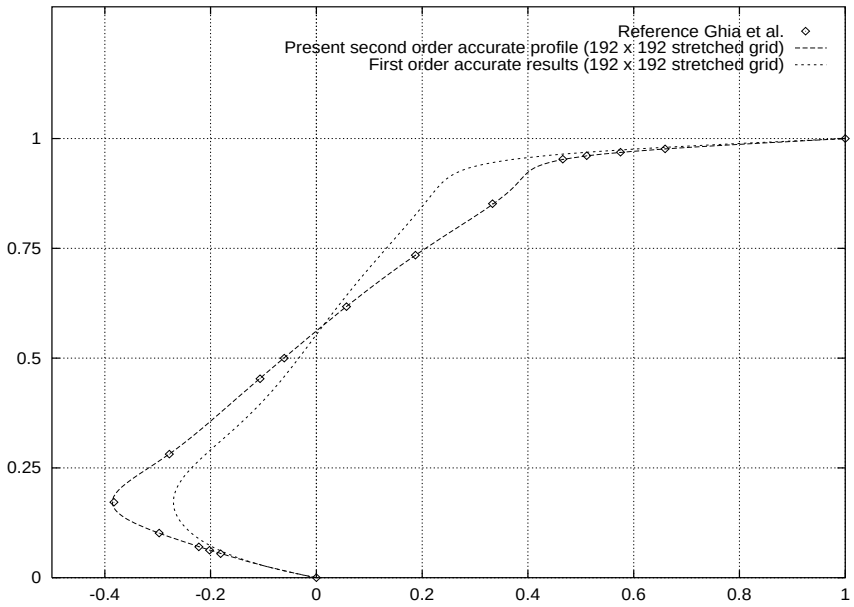

Figure 15: The u-centerline velocity profile for first and second order accurate discretizations versus reference values from [9].

coupled collective alternating tri-line smoother, which means that the three unknowns belonging to a grid point are smoothed simultaneously. For line smoothers this means that not only a tri-diagonal system, but a system with more diagonals (referring to all unknowns on the line) is solved in a smoothing iteration. (Since we choose $\kappa = 0$ we have identical smoothers from Splitting 1 and Splitting 2 and the discretization from (47) is in the left-hand side of the KAPPA smoothers. The underrelaxation parameters are the same as presented above: $\omega = 1$ for the symmetric and $\omega = 0.7$ for the tri-line smoother). Because of the rotating problem we perform F-cycles. For the symmetric smoother F(1,0)-cycles are used, while for the tri-line smoother F(1,1)-cycles are used. Note that the alternating tri-line smoother is now twice as expensive as the alternating symmetric smoother. The convergence of the residual $\sum_{i=1}^{ieq} |r^{i(m)}|_\infty$, (where the number of equations $ieq = 3$) is presented in Figure 16, where we also compare the coarse grid discretization with L_2 and with L_1.
It can be seen that a very fast multigrid convergence is obtained for this test problem with the alternating symmetric KAPPA smoother with L_2-coarse grid discretizations. Here, a difference in convergence can be observed between choosing L_1 or L_2 as coarse grid discretization: Choosing L_2 results in fastest convergence. Also the difference between the symmetric and the tri-line smoother is clear, but the worst convergence presented here is still very satisfactory. We give the wall-clock times needed to perform the computations that lead to the curves in Figure 16 which is the time to perform 10 multigrid cycles plus FMG for the starting solution on the finest grid. The timings are performed on a single RS6000 workstation. For 10 F(1,0)-cycles (+ FMG) with the symmetric collective smoother and the L_2 coarse grid discretization 398 seconds are needed, for 10 F(1,0)-cycles with L_1 coarse discretizations 322 seconds are needed; the 10 F(1,1)-cycles with the tri-line collective smoother and L_2 coarse grid discretizations took 700 seconds and with L_1 coarse discretizations took 570 seconds.

Finally, we would like to show the convergence with increasing grid sizes for this problem with the symmetric alternating line smoother and the full second order formulation. Therefore we here

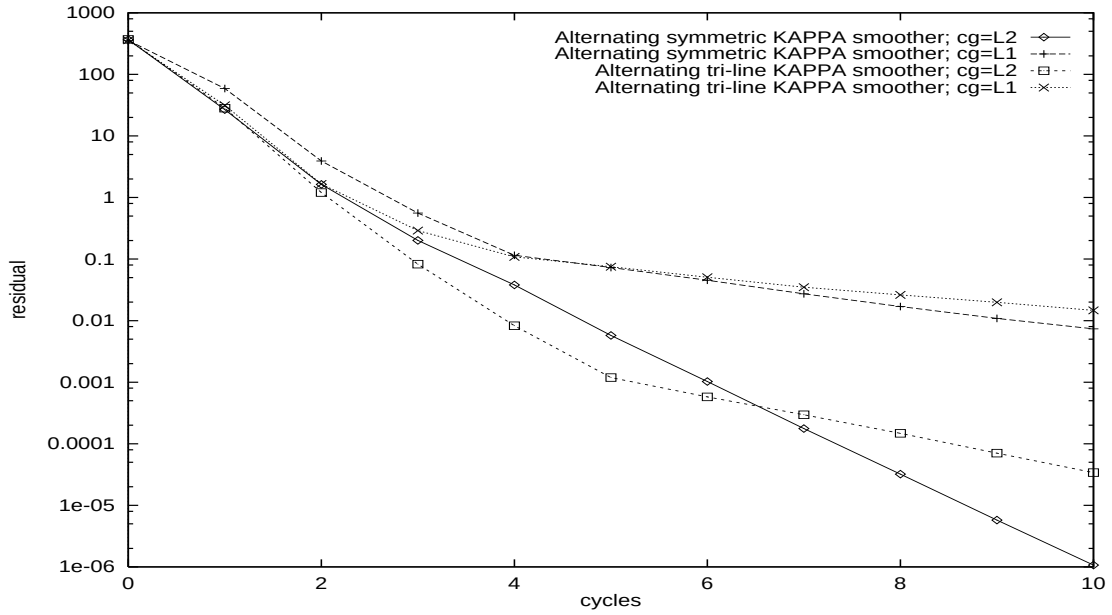

Figure 16: The multigrid convergence for the driven cavity problem ($Re = 1000$) with the alternating symmetric and the alternating tri-line smoother, 192×192 stretched grid.

consider the convergence on $64^2, 128^2$ and 256^2 grids without stretching. In Table VII the number of iterations needed to reduce the initial residual by 6 orders of magnitude is presented, and within brackets the corresponding wall-clock time (the FMG stage included). Due to improving

grid:	# its.	wall-clock time (s)
64^2	15	(58.0)
128^2	10	(156.0)
192^2	8	(284.0)
256^2	8	(505.0)

Table VII: Number of iteration and wall-clock time (s) for reducing the initial residual by 6 orders of magnitude, driven cavity problem at $Re = 1000$.

mesh-Reynolds numbers (local ratio between convection and diffusion) the convergence improves for increasing grid sizes, as can be seen in Table VII. The single grid convergence for this problem is very poor; the wall-clock times are not comparable to the multigrid wall-clock times.

4.5 An Euler channel flow problem

A last example is compressible Euler flow in a channel with a bump. The 2D steady compressible Euler equations are written in their differential form as follows,

$$\frac{\partial f(\mathbf{u})}{\partial x} + \frac{\partial g(\mathbf{u})}{\partial y} = \frac{\partial}{\partial x}\begin{bmatrix} \rho u \\ \rho u^2 + p \\ \rho uv \\ (E+p)u \end{bmatrix} + \frac{\partial}{\partial y}\begin{bmatrix} \rho v \\ \rho uv \\ \rho v^2 + p \\ (E+p)v \end{bmatrix} = 0$$

$$p = (\gamma - 1)(E - \frac{1}{2}\rho(u^2 + v^2)), \tag{48}$$

ρ is the density, u and v the Cartesian velocity components, E the total energy, p the pressure, and γ (assumed to be constant) is the ratio of the specific heats at constant pressure and constant volume.
The vertex-centered finite volume discretization adopted for the Euler equations is described briefly. It is based on the cell-centered discretization in [18], [13]. For the finite volume discretization the domain Ω is divided into control volumes $\Omega_{i,j}$. For each quadrilateral (48) must hold in integral form:

$$\oint_{\partial\Omega_{i,j}} (f(\mathbf{u})n_x + g(\mathbf{u})n_y)dS = 0 \tag{49}$$

where $(n_x, n_y)^T = (cos\phi, sin\phi)^T$ is the outward normal vector on $\partial\Omega_{i,j}$, and $\mathbf{u}$ is the state vector. The rotational invariance of the Euler equations is used, and the discretization results in:

$$\sum_{(ik)\in k(ik)} F(\mathbf{u}^L, \mathbf{u}^R)\partial S_{ik} = 0 \tag{50}$$

with $k(ik)$ being the set of neighboring cells of $\Omega_{i,j}$; ∂S_{ik} is the length of the boundary between $\Omega_{i,j}$ and Ω_{ik}; $F(\mathbf{u}^L, \mathbf{u}^R)$ is an approximate Riemann solver, which depends on the left, $\mathbf{u}^L$, and right state, $\mathbf{u}^R$, along the cell boundary. The discretization requires a calculation of the convective flux at each cell face $\partial S_{i,j}$. The approximate solution $F(\mathbf{u}^L, \mathbf{u}^R)$ of the 1D Riemann problem is solved with an approximate Riemann solver proposed by Osher in its P-variant (for more details see [18], [13]):

$$F(\mathbf{u}^L, \mathbf{u}^R) = \frac{1}{2}(\tilde{f}(\mathbf{u}^L) + \tilde{f}(\mathbf{u}^R) - \int_{\mathbf{u}^L}^{\mathbf{u}^R} |A(\mathbf{u})|d\mathbf{u}) \tag{51}$$

where $|A(\mathbf{u})|(= A^+(\mathbf{u}) - A^-(\mathbf{u}))$ is a splitting of the Jacobian matrix A into matrices with positive and negative eigenvalues, and $\tilde{f}$ is the one-dimensional flux along the normal vector. State vector $\mathbf{u} = (u, v, c, z)^T$ is chosen, where $c \equiv \sqrt{\gamma p/\rho}$ is the speed of sound and $z \equiv ln(p\rho^{-\gamma})$ is an unscaled entropy.
The states $\mathbf{u}^L_{i+\frac{1}{2},j}$ and $\mathbf{u}^R_{i+\frac{1}{2},j}$ in (51) are approximated by a discretization with van Leer limiter (8), in order to avoid oscillations that may appear near shocks.

A transonic problem ($Ma = 0.85$) in a channel with a bump is evaluated. The bump in the channel is a 4.2% circular bump, the height of the channel is 2.1. Its length is 5, the bump length is 1. The pressure distribution of the transonic test is presented in Figure 17. The domain is discretized with 96×64 cells, which results in a multigrid method with 5 levels. With

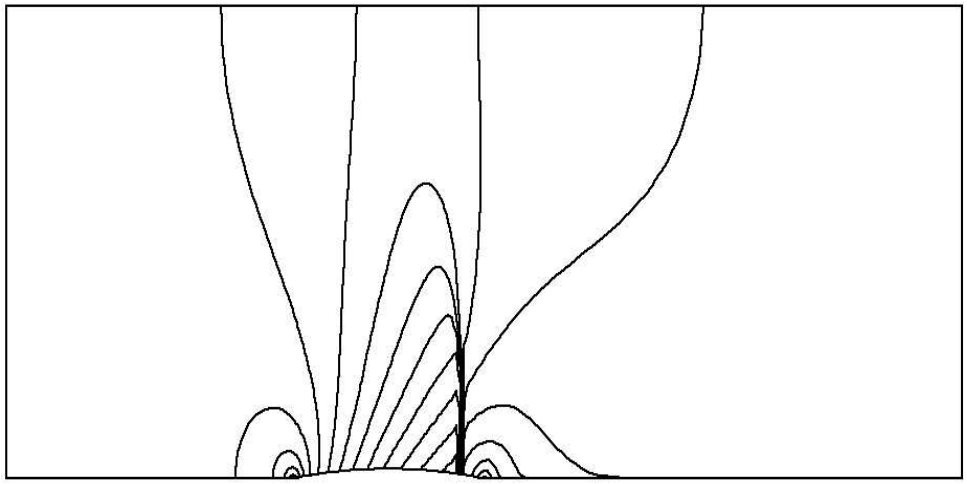

Figure 17: The pressure distribution for the transonic test $Ma = 0.85$, 96×64-grid.

the smoother from Splitting 2 the second order discretization for the Euler equations is solved directly with V(2,1)-cycles. The smoother from Splitting 2 showed the best convergence results for discretization with limiters from class 1. Again we compare the multigrid performance with coarse grid discretizations based on L_2 with L_1 and the alternating symmetric smoother with the alternating tri-line smoother ($\omega = 0.7$). Figure 18 presents the convergence: $\sum_{i=1}^{ieq} |r^{i(m)}|_\infty$ with $ieq = 4$ and m the multigrid iteration.
For this Euler test, where a shock appears in the solution, similar convergence is obtained as for the scalar problems with the van Leer limiter. It appears to be best for this test problem also to adopt the L_2 discretization on the coarse grids. The convergence is very satisfactory for both, the alternating symmetric and the alternating tri-line smoother. Table VIII presents the number of iterations to reduce the initial residual by 6 orders of magnitude plus corresponding wall-clock time on different grids. Here we would like to mention that the flux difference splitting is not implemented in the most efficient way, which strongly infuences the wall-clock times. One can

grid:	# its.	wall-clock time (s)
48×32	10	(123.0)
96×64	11	(511.0)
192×128	10	(1844.0)

Table VIII: Number of iteration and wall-clock time (s) for reducing the initial residual by 6 orders of magnitude, transonic Euler channel problem at $Ma = 0.85$.

observe level independent convergence from Table VIII for this transonic Euler problem. Here, the single grid convergence is poor and not comparable to the multigrid convergence.

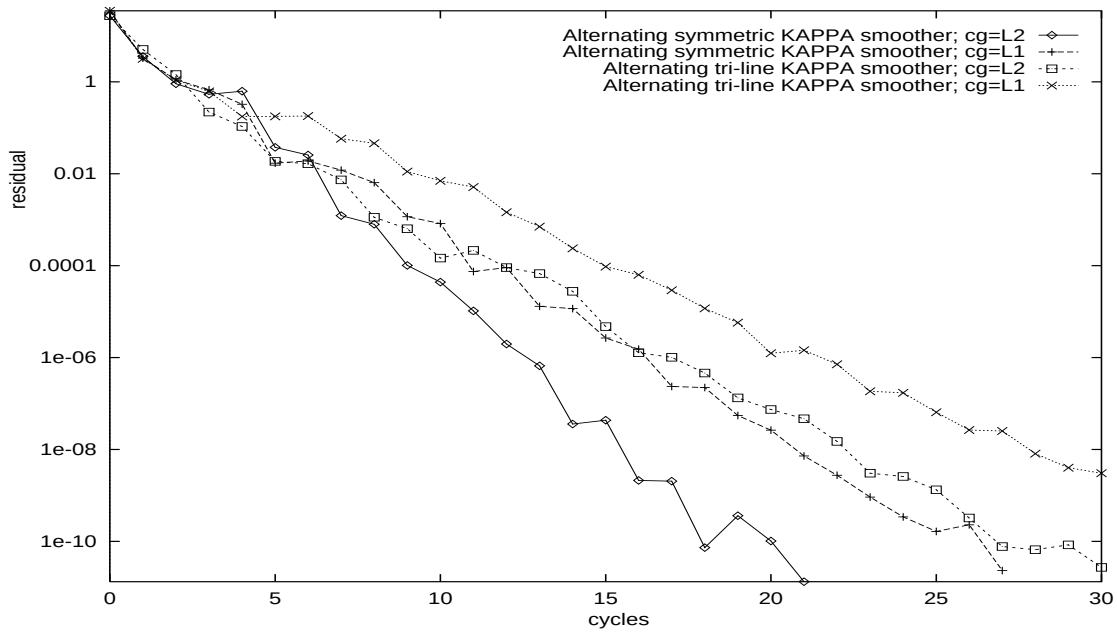

Figure 18: The multigrid convergence for a transonic Euler example ($Ma = 0.85$) with the alternating symmetric and the alternating tri-line smoother, 96×64 stretched grid.

5 Conclusion

We have presented KAPPA smoothers for convection-dominated problems. The smoothers are based on a splitting into a 'positive' part in the left-hand side and a remaining part in the right-hand side. For linear κ-discretizations, we have performed Fourier analysis for a convection-dominated convection-diffusion equation in order to study the multigrid convergence behavior theoretically. Furthermore, a parallel variant is presented and evaluated. In general, it is preferable to use the line smoothers based on lexicographical ordering compared to the tri-line variant. The KAPPA smoothers show a very promising multigrid convergence with linear κ-discretizations, not only for convection-diffusion problems, but also for an incompressible Navier-Stokes flow problem. Next to linear κ-discretizations also TVD discretizations with limiters are evaluated for 'difficult' scalar equations and for a compressible Euler channel flow problem. Also here the convergence presented is very satisfactory: The reduction of the residual from the higher order discretization is remarkable. We could observe a fast and robust convergence for several problems, especially for discretizations with limiters from class 1. The single grid convergence for the scalar convection-dominated problems is also satisfactory on not too fine grids. Many tests with two different splittings, choosing the coarse grid discretization with the first order or the second order discretization, and the comparison between the alternating symmetric and the alternating tri-line smoother gave much insight in the behavior of the smoothers.

References

[1] D. Bradly, M. Missaghi and S.B. Chin, A Taylor-series approach to numerical accuracy and a third-order scheme for strong convective flows. *Comp. Meth. Appl. Mech. Engng.*, **69,** 133-155 (1988).

[2] A. Brandt, Multi–level adaptive solutions to boundary–value problems. *Math. Comp.* **31**, 333–390 (1977).

[3] A. Brandt and I. Yavneh, On multigrid solution of high-Reynolds incompressible entering flows. *J. Comp. Phys.* **101,** 151–164 (1992).

[4] A. Brandt and I. Yavneh, Accelerated multigrid convergence and high-Reynolds recirculating flows. *SIAM J. Sci. Comp.*, **14,** 607–626 (1993).

[5] J-A. Desideri and P.W. Hemker, Convergence analysis of the defect-correction iteration for hyperbolic problems. *SIAM J. Sci. Comp.*, **16,** 88–118 (1995).

[6] E. Dick and J. Linden, A multigrid method for steady incompressible Navier-Stokes equations based on flux difference splitting. *Int. J. Num. Methods in Fluids* **14,** 1311–1323 (1992).

[7] E.Dick and K. Riemslagh, Multi-staging of Jacobi relaxation to improve smoothing properties of multigrid methods for steady Euler equations. *J. Comp. Appl. Math.*,**50,** 241–254 (1994).

[8] P.H. Gaskell and A.K.C. Lau, Curvature-compensated convective transport: SMART, a new boundedness-preserving transport algorithm. *Int. J. Num. Meth. Fluids,* **8,** 617–641 (1988).

[9] U. Ghia, K.N. Ghia and C.T. Shin, High-Re solutions for incompressible flow using the Navier-Stokes equations and a multigrid method. *J. Comp. Phys.* **48,** 387–411 (1982).

[10] W. Hackbusch, *Multi-grid methods and applications.* Springer, Berlin (1985).

[11] Ch. Hirsch, *Numerical computation of internal and external flows,* Vol. 2. John Wiley, Chichester (1990).

[12] A. Jameson, W. Schmidt and E. Turkel, Numerical simulation of the Euler equations by finite volume methods using Runge-Kutta time stepping schemes. *AIAA*-81-1259 (1981).

[13] B. Koren, Defect correction and multigrid for an efficient and accurate computation of airfoil flows. *J. Comp. Phys.*, **77**, 183–206 (1988).

[14] B. Koren, A robust upwind discretization method for advection, diffusion and source terms. *In:* C.B. Vreugdenhil and B. Koren (eds.), *Numerical methods for advection-diffusion problems*, Notes on Num. Fluid. Mech., Vieweg Braunschweig 117–137 (1993).

[15] C.W. Oosterlee and T. Washio, *An evaluation of parallel multigrid as a solver and a preconditioner for singular perturbed problems, Part I The standard grid sequence.* GMD Arbeitspapier 980, St. Augustin, Germany (1996). To appear in SIAM SISC.

[16] D. Sidilkover and A. Brandt, Multigrid solution to steady-state two-dimensional conservation laws. *SIAM J. Num. Anal.*, **30** 249–274 (1993).

[17] R.M. Smith and A.G. Hutton, The numerical treatment of advection: A performance comparison of current methods. *Num. Heat Transfer,* **5,** 439–461 (1982).

[18] S.P. Spekreijse, *Multigrid solution of the steady Euler equations*, CWI Tract 46, CWI Amsterdam (1988).

[19] J.Steelant, S. Pattijn and E. Dick, Smoothing properties of different preconditioners for Navier-Stokes equations. *Proceedings 3rd ECCOMAS* Conf. on Comp. Fluid Dynamics. 616–621 (1996).

[20] K. Stüben and U. Trottenberg, Multigrid methods: fundamental algorithms, model problem analysis and applications. *In:* W.Hackbusch, U. Trottenberg (eds.), *Multigrid Methods*, Lecture Notes in Math. **960,** 1–176, Springer, Berlin, Germany (1982).

[21] B. van Leer, Upwind-difference methods for aerodynamic problems governed by the Euler equations. In: B. Enquist, S. Osher, R. Somerville (eds.), *Large scale computations in fluid mechanics.* Lectures in Applied Mathematics, Vol. 22, II, Americ. Math. Soc., Providence, R.I., 327-336 (1985).

[22] R.S. Varga, *Matrix iterative analysis.* Prentice-Hall, Englewood Cliffs, N.J. (1962).

[23] T. Washio and C.W. Oosterlee *Flexible multiple semicoarsening for three-dimensional singularly perturbed problems.* GMD Arbeitspapier 1012, GMD St. Augustin, Germany (1996). To appear in SIAM SISC 1998.

[24] P. Wesseling, *An introduction to multigrid methods.* John Wiley, Chichester (1992).

[25] M. Zijlema, *Computational modelling of turbulent flow in general domains.* Ph.D. Thesis, Techn. University Delft, The Netherlands (1996).